# Identifying Resonant Dopants for $BaCu_2S_2$ from First Principle Calculations for Thermoelectric Applications

**A Thesis**

submitted to
Indian Institute of Science Education and Research Pune
in partial fulfillment of the requirements for the
BS-MS Dual Degree Programme

by

**Mohamed Hashim K**


Indian Institute of Science Education and Research Pune
Dr. Homi Bhabha Road,
Pashan, Pune 411008, INDIA.

May, 2021

Supervisor: Prof. Prasenjit Ghosh, Department of Physics

This thesis is dedicated to my parents

# Certificate

This is to certify that the work contained in the thesis entitled "**Identifying Resonant Dopants for $BaCu_2S_2$ from First Principle Calculations for Thermoelectric Applications**" towards partial fulfillment of the BSMS dual degree programme at the Indian Institute of Science Education and Research, Pune has been carried out by Mohamed Hashim under the supervision of Prof. Prasenjit Ghosh, during the period of Aug 2020-June 2021.

Prasenjit Ghosh
Associate Professor
Department of Physics
IISER Pune

# Declaration

I hereby declare that the work contained in this dissertation titled "**Identifying Resonant Dopants for $BaCu_2S_2$ from First Principle Calculations for Thermoelectric Applications**" has been carried out by me at the Department of Physics, Indian Institute of Science Education and Research, Pune, under the supervision of Prof. Prasenjit Ghosh. The content of the thesis has not been submitted elsewhere for any other degree.

Mohamed Hashim
20161104
BSMS
IISER Pune

# Acknowledgement

I would like to first thank my supervisor, Prof. Prasenjit Ghosh, for his continuous guidance and motivation throughout the project. I am grateful to him for being patient and understanding at difficult times. I am indebted to him for his precious time and insightful teachings. I also would like to thank my TAC member Prof. Surjeet Singh for the suggestions and the feedbacks. I would like to thank Gautam Sharma for the constant assistance whenever needed. I also would like to thank my family, all the friends, labmates for giving me support and advice during the work.

# Abstract

Distortion of the density of states(DOS) via resonant level has been reported to improve the thermoelectric figure of merit (ZT) of material. $BaCu_2S_2$ exists in two phases a high-temperature tetragonal phase and a low-temperature orthorhombic phase. In this study, we tried doping various elements(Al, Ga, In, Tl, As, and Sb) at different sites of both phases. For the lowest formation energy configurations, we further explored the effect of various dopants in the electronic structure of the compound. Some of the dopants created new defect states overlapping with the parent states(resonant level), close to the band edge. Tl created defect states in both the VB and CB band edges. Studied the thermoelectric properties of dopants. Group 13 dopants in the orthorhombic phase showed a carrier concentration-dependent improvement in Seebeck coefficients for both the holes and electrons due to the resonant level.

# Contents

# Chapter 1

# Introduction

## 1.1 Thermoelectric Materials

Thermoelectric materials are useful in conversion of heat into electric current and vice versa. Their application includes waste-heat recovery, thermoelectric coolers etc. They are simple, cheap and reliable to use, which makes them irreplaceable by any conventional methods. But the low efficiency of conversion between heat and electricity is the major drawback of any thermoelectric material.

Thermoelctric effect constitutes Seebeck, Peltier and Thomson effects. Seebeck effect refers to conversion of temperature difference into voltage difference, Peltier effect refers to conversion of voltage difference to temperature difference, and Thomson effect refers to reversible cooling or heating in a conductor under both temperature and voltage gradient. Its application varies from refrigeration to power generation (Figure: 1.1). The efficiency of a thermoelectric material is measured by an unit less quantity called the Figure of Merit (ZT), which can be written as,

$$ZT = \frac{S^2 \sigma T}{\kappa} \tag{1.1}$$

where $S$ is the Seebeck coefficient, $\sigma$ is the electrical conductivity, $T$ is the temper-

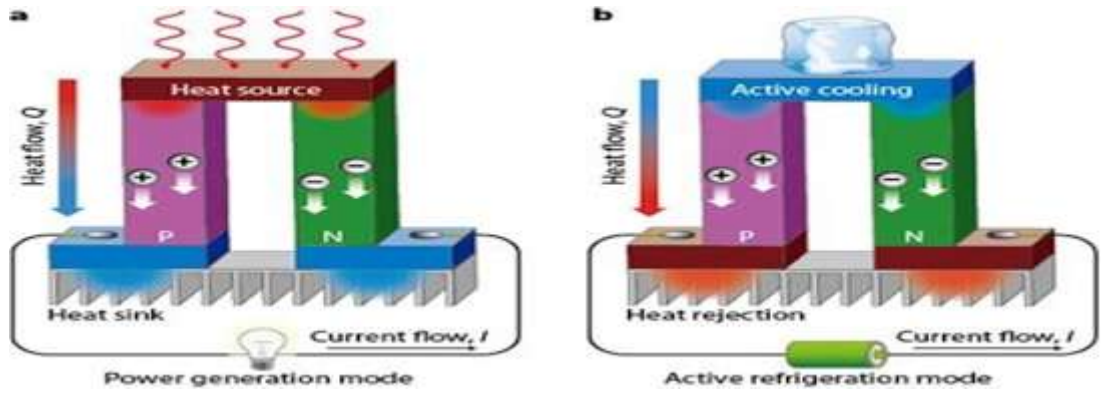


Figure 1.1: Power generation and Peltier cooling of a thermoelectric("Evaluation of a PV-TEG Hybrid System Configuration for an Improved Energy Output: A Review", Umar Abubakar Saleh, licensed under CC-BY-SA 4.0 [25])

ature, $\kappa$ is the thermal conductivity and includes both lattice thermal conductivity ($\kappa_L$) and electronic contribution to thermal conductivity ($\kappa_e$).

The major problem in improving the ZT is due to the counteracting nature of its various component, which means a mechanism that improve one component might deteriorate the other[4]. But the lattice thermal conductivity ($\kappa_L$) is nearly independent of the other quantities involved. So a variety of attempts have been made to decrease $\kappa_L$ keeping other quantities intact, like low sound velocity[26], but there is a limit for reducing the $\kappa_L$, known as the amorphous limit[24]. The other quantities like S, $\sigma$, $\kappa_e$ are dependent on the electronic structure of a material. So different types of techniques have been explored for improving those quantities like band convergence[20], resonant levels[4], etc.

## 1.2 Resonant Doping

Resonant doping is a band engineering technique to improve the electronic contribution, $S^2\sigma$, of the figure of merit. Here we will discuss the phenomenon of resonant doping or resonant level and its role in the enhancement of figure of merit of a material($BaCu_2S_2-$phase).

### 1.2.1 Resonant states or virtual bound states

If the new dopant state is degenerate with continuum of the energy spectrum of the parent crystal, it is called as resonant state. So all the impurity states in zero-gap semiconductors, metals are resonance states. In a finite band-gap semiconductor, if the defect level is in bandgap, as in classical dopant which provides free charge carriers, one can activate the carrier by providing activation energy ($E_D$), which is effectively modelled by hydrogenoid model. It is also possible to have resonant state in finite gap semiconductors (where the $E_D$ is negative) (Figure:1.2).

Since the resonant state and the extended state have the same energy level, they resonate to create a closely lying two new extended states, which in turn resonate with the corresponding extended states. So consequently the resonant state builds some width $\Gamma$. One can describe resonant state mathematically as following.

Unperturbed parent state can be represented by,

$$H_0 \left|\vec{k}\right\rangle = E_k \left|\vec{k}\right\rangle \tag{1.2}$$

where $\vec{k}$ is the wave vector and the Hamiltonian for isolated dopant atom can be written as

$$H_{at} \left|O\right\rangle = E_0 \left|O\right\rangle \tag{1.3}$$

where $|O\rangle$ are atom-like eigenstates denoted by an orbital quantum number. If $E_0$ falls over an extended state, resonance happens. A new perturbed Hamiltonian can be written as $H = H_0 + V$, which takes into account their interaction. So the new

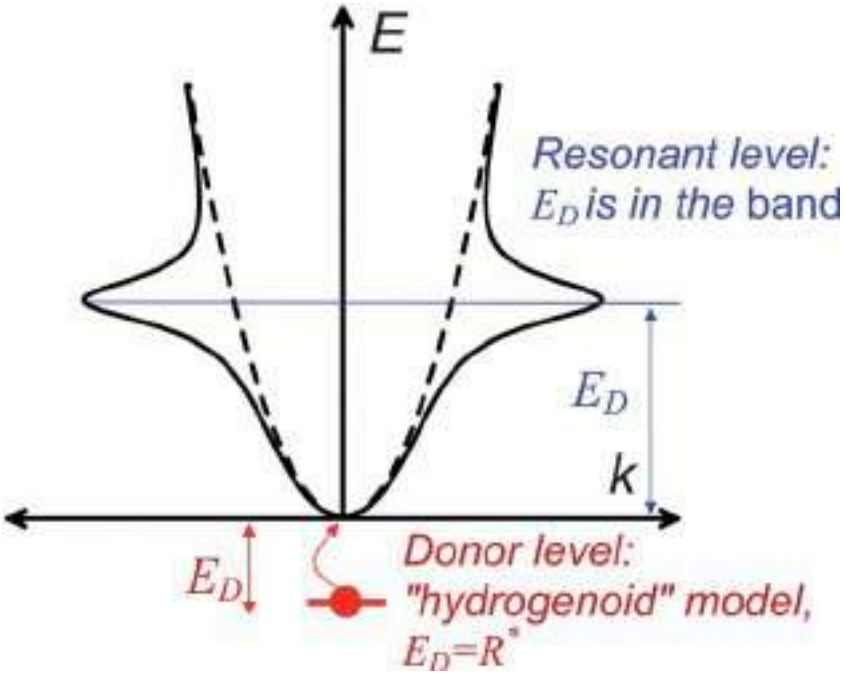


Figure 1.2: Resonant state and classical dopant state in band structure(Reprinted with permission from ref.[4] Copyright 2018, Energy & Enviornmental Science)

eigenstate $|\psi\rangle$can be written as[4].

$$\begin{aligned} H\,|\psi\rangle &= E\,|\psi\rangle \\ |\psi\rangle &= c\,|O\rangle + \int\int\int a(\vec{k})\,|\vec{k}\rangle\,d^3k \end{aligned} \tag{1.4}$$

Solving this will provide the amount of impurity present in a new eigenstate after doping. The coefficient of impurity state $c$ in eq(1.4) is given by

$$\begin{aligned} |c|^2 &= \frac{|\,\langle O|V|k\rangle\,|^2}{(E-E_0-\Delta)^2+(\frac{\Gamma}{2})^2} \\ \Gamma &= 2\pi|\,\langle O|V|k\rangle\,|^2 g(E) \end{aligned} \tag{1.5}$$

where $g(E)$ is the DOS of the extended host material. Since a dopant atom consists of different energy level, it is possible to get some resonant level upon doping. But the position with respect to Fermi level and width of a resonant state ($\Gamma$) are crucial for thermoelectric applications. Heremens *et al* has pointed out some necessary criteria for a resonant level for optimal ZT improvement[4].

### 1.2.2 Resonant doping and thermoelectric property

Mahan and Sofo[12] suggested that the narrowest energy distribution of states with high carrier velocity (along applied electric field) near Fermi level will maximize the thermoelectric figure of merit. But this has some practical limitations like, hard to position Fermi level, large Wigner-delay time (time spent by a carrier near resonant center) for narrow distribution, and presence of background DOS. A resonant level

modifies the thermoelectric property of a material by distorting the density of state or through resonant scattering

### DOS distortion

One can expand the equation of Seebeck for the single-band case with Bathe-Sommerfield expansion, as follows[4]

$$\begin{aligned} S &= \frac{\pi^2}{3}\frac{k_B}{q}(k_B T)\left(\frac{1}{n(E)}\frac{dn(E)}{dE} + \frac{1}{\mu(E)}\frac{d\mu(E)}{dE}\right) \\ S &= \frac{\pi^2}{3}\frac{k_B}{q}(k_B T)\left(\frac{1}{n}\frac{g(E)}{dE} + \frac{1}{\mu(E)}\frac{d\mu(E)}{dE}\right) \end{aligned} \tag{1.6}$$

where $k_B$ is the Boltzmann constant, g(E) is the DOS, $\mu$ is the mobility of carrier, $n$ is the integral of g(E) over E. The increased DOS near the Fermi level will improve the Seebeck coefficient directly through $g(E)$ term. The effect of $g/n$ term has a larger impact on semiconductor materials due to very low carrier concentration. The increased $g(E)$ also reduces the velocity of carriers[17]. The second term in eq(1.6), which depends on the width of the peak, gets affected by an "effective energy-filtering mechanism" or "resonant doping"[4]. The effect of resonant scattering is more pronounced at cryogenic temperature. Reduction of mobility is also observed in resonant doping, which also increases the second term of eq(1.6). The aforementioned effect of resonant doping are the ones, beneficial for a material's thermoelectric property. But there are other effects due to resonant doping like fermi level pinning-if the resonant state is due to a very localized orbital of dopant, eg Ti in PbTe[9]. Even though there are many examples of localized resonant levels in a semiconductor, only few of them have improved the Seebeck coefficient (mentioned the criteria for a resonant level to improve the ZT before). Signature of a resonant level in Seebeck can be observed with a deviation from the parent behavior upon doping in Seebeck vs carrier concentration plot(depends on both on the temperature and carrier concentration)[17][30].

## 1.3 Aim of this thesis

As part of this work, we would like to identify the possible resonant dopants for $BaCu_2S_2$, which might increase the $S^2\sigma$ of the material using first-principle calculations. $BaCu_2S_2$ can be found in two phases, low temperature orthorhombic and high temperature tetragonal. We have studied both the phases. The transition from orthorhombic to tetragonal happens around 820K[15]. Both are semiconductors with some good properties for potential thermoelectric material. Orthorhombic phase has got the large value of Seebeck coefficient of about 450-550$\mu V/K$ near room temperature[15]. A very low thermal conductivity 0.86 $Wm^{-1}K^{-1}$, less than that of the state-of-the-art material has been reported for the tetragonal phase and a ZT of 0.17 has been reported. Both tetragonal and orthorhombic are p-type materials, i.e holes are the major carriers. The origin of holes was due to presence of copper vacancies.

The dopants tried were Group 13 elements, i.e., Al, Ga, In, Tl and two group 15 elements, As, Sb. Some of them have been reported for improving thermoelectric figure of merit due to resonant doping in other materials like In in GeTe. The average ZT got increased by 70% on In doping in GeTe[30]. All the above dopants show multivalency - a property identified in all reported resonant dopants. Identifying a resonant dopant that works in both phases is more beneficial from an application point of view as in In doping in rhombohedral and cubic GeTe[30]. Since these are semiconductors, the suitable resonant state would be from $s$ and $p$ orbital of dopants [4].

# Chapter 2

# Theoretical and Computational Methods

The electronic structure of a material gives insight into its structural, mechanical and transport properties. We have used Density Functional Theory, a quantum mechanical method for calculating the electronic structure of the material. We have extracted the transport properties using semi classical Boltzmann transport theory[11], with the information obtained from the electronic structure calculations.

## 2.1 Many Body Schrodinger Equation

We can write the time-independent Schrodinger equation as

$$\hat{H}_{tot}\Psi_{tot} = E_{tot}\Psi_{tot} \tag{2.1}$$

where the many body wave function $\Psi_{tot}$ is a function of position of all the electrons ($\mathbf{r}$) and nuclei ($\mathbf{R}$) constituting the system, $\Psi_{tot}(\mathbf{r}, \mathbf{R})$. $\hat{H}_{tot}$ is the Hamiltonian of the system and can be written as [2]

$$\begin{aligned}\hat{H}_{tot} = -\sum_{i=1}^{N}\frac{\hbar^2}{2M_i}\nabla_i^2 - \sum_{j=1}^{N}\frac{\hbar^2}{2m_j}\nabla_j^2 + \frac{1}{4\pi\epsilon_0}\frac{(Ze)^2}{2}\sum_{i,i'}\frac{1}{|R_i - R_i'|} + \\ \frac{1}{4\pi\epsilon_0}\left(\frac{e^2}{2}\sum_{j,j'}\frac{1}{|r_j - r_j'|} - ze^2\sum_{i,j}\frac{1}{|r_j - R_i|}\right)\end{aligned} \tag{2.2}$$

where $-\sum_{i=1}^{N}\frac{\hbar^2}{2M_i}\nabla_i^2$ and $-\sum_{j=1}^{N}\frac{\hbar^2}{2m_j}\nabla_j^2$ are kinetic energies of nuclei and electrons respectively, $\frac{1}{4\pi\epsilon_0}\frac{(Ze)^2}{2}\sum_{i,i'}\frac{1}{|R_i - R_i'|}$ and $\frac{1}{4\pi\epsilon_0}\frac{e^2}{2}\sum_{j,j'}\frac{1}{|r_j - r_j'|}$ are Coulomb interaction between nuclei-nuclei and electron-electron respectively and the last term $\frac{1}{4\pi\epsilon_0}Ze^2\sum_{i,j}\frac{1}{|r_j - R_i|}$ is the Coulomb interaction between nuclei and electron. $\Psi_{tot}$ contains all the information about the system. The non-local electron-electron and electron-nuclei interaction terms in (2.2) makes it difficult to solve the equation analytically. Various approximation have been made to solve it.

## 2.2 Born-Oppenheimer Approximation

The equation (2.2) can be written as,

$$[T_N + T_e + V_{NN} + V_{ee} + V_{Ne}]\Psi_{tot}(\mathbf{r}, \mathbf{R}) = E_{tot}\Psi_{tot}(\mathbf{r}, \mathbf{R}) \tag{2.3}$$

Here $T_N$ is the nucleus kinetic energy, $T_e$ is the kinetic energy of electron,$V_{NN}$, $V_{ee}$, $V_{eN}$ are the nucleus-nucleus, electron-electron and electron-nucleus Coulombic interactions respectively.

Nuclear motion is much slower than the electron due to its heavier mass(nearly 2000 $M_e$). This means the electron wave function depends only on nuclear position, not its velocity, and the nucleus experiences a smeared out potential from the speedy electron. This is the Born-Oppenheimer approximation, which gives an electronic state, that is independent of nuclear motion.[2]
We can identify the Hamiltonian in equation (2.3) as

$$\hat{H}_{tot} = \hat{H}_N + \hat{H}_{ele}$$

where $\hat{H}_{ele} = T_e + V_{Ne} + V_{ee}$ and $\hat{H}_N = T_N + V_{NN}$, $\hat{H}_{ele}$ is a function of electronic coordinates, and has parametric dependence on nuclear coordinates. $\hat{H}_N$ is the function of nuclear coordinates. This allows decoupling of total wave function into

$$\Psi_{tot}(\mathbf{r}, \mathbf{R}) = \Phi_e(\mathbf{r}; \mathbf{R})\Phi_N(\mathbf{R}) \tag{2.4}$$

Then the Schrodinger equation for electrons, for fixed nuclear coordinates become,

$$\hat{H}_{ele}\Phi_e(\mathbf{r}; \mathbf{R}) = E_{ele}(\mathbf{R})\mathbf{\Phi_e}(\mathbf{r}; \mathbf{R}) \tag{2.5}$$

The ionic part can be obtained by substituting equation (2.5) in (2.3).

$$(\hat{H}_N + E_{ele}(\mathbf{R}))\Phi_N(\mathbf{R}) = E_{tot}\Phi_N(\mathbf{R}) \tag{2.6}$$

In effect, the nuclei move in the potential energy surface created by all the electrons $E_{ele}(\mathbf{R})$). Due to large mass of nucleus, it can be considered as a classical particle then the equation of motion for nuclei can be derived by invoking Newton's law and solving a 2nd order differential equation or one can get the equilibrium nuclear coordinates by finding the minimum of the potential energy surface $E_{ele}(\mathbf{R})$) w.r.t nuclear coordinates.

## 2.3 Hohenberg-Kohn Theorems

Even with the static nuclei approximations, equation (2.5) is hard to solve analytically due to the electron-electron interaction term. Here the Density functional theorem comes in handy proposed by Kohn and Hohenberg. They proposed to use electron density as the basic variable instead of the wavefunction, which drastically reduces the degrees of freedom in the system (from 3N variables to 3). Hohenberg-Kohn theorems represents the basis of density funcitonal theory.

**Theorem 1**: "For any system of interacting particles, external potential $V_{ext}(r)$ is an unique functional of ground state density $n(r)$ and vice-versa," [5] [27] where $n(r)$ is defined as

$$n(r) = N \int \int .. \int |\Psi(\mathbf{r_1}, \mathbf{r_2}, .., \mathbf{r_n})|^2 d^3\mathbf{r_1} d^3\mathbf{r_2} .. d^3\mathbf{r_N} \tag{2.7}$$

The proof is based on the proof by contradiction. Consider two external potentials $V_{ext}$ and $V'_{ext}$, which vary by other than a constant and provides with the same ground state electron density $n(r)$. Then the respective Hamiltonian would be $H$, $H'$ with different normalised ground state electronic wavefunctions $\Psi_0$ and $\Psi'_0$, with the energy eigenvalue $E_0$ and $E'_0$

$$E_0 < \langle \Psi'_0 | H | \Psi'_0 \rangle = \langle \Psi'_0 | H' | \Psi'_0 \rangle + \langle \Psi'_0 | H - H' | \Psi'_0 \rangle \tag{2.8}$$

$$E_0 < E'_0 + \langle \Psi'_0 | T + V_{ee} + V_{ext} - T - V_{ee} - V'_{ext} | \Psi'_0 \rangle \tag{2.9}$$

$$E_0 < E'_0 + \int n(\mathbf{r}) \{V_{ext} - V'_{ext}\} d\mathbf{r} \tag{2.10}$$

Similarly,

$$E'_0 < E_0 - \int n(\mathbf{r}) \{V_{ext} - V'_{ext}\} d\mathbf{r} \tag{2.11}$$

adding eq(2.9) and (2.10), leaves us with a clear contradiction,

$$E_0 + E'_0 < E_0 + E'_0 \tag{2.12}$$

This summarizes the proof that there cannot be two different external potentials giving rise to the same ground-state electron density or in other words ground state density uniquely determines the external potential $V_{ext}$.

$$n_0(r) \implies \hat{H} \implies \Psi \implies E_0$$

$$E[n_0] = T[n_0] + E_{ee}[n_0] + E_{ext}[n_0] \tag{2.13}$$

The total energy functional $E[n_0]$ constitutes of the functionals of kinetic energy $T[n_0]$, electron-electron interaction energy $E_{ee}[n_0]$ and energy functional due to the external potential $E_{ext}[n_0]$. So the complete ground state energy or its components are functionals of ground state electron density. It is convenient to seperate the energy expression (2.13) into parts which depends on actual system. That is the potential energy due to nuclei electron attraction $E_{ext}[n_0] = \int n_0(\mathbf{r}) V_{ext} d\mathbf{r}$ and those with the universal form.

$$E[n_0] = \left( \int n_0(\mathbf{r}) V_{ext} d\mathbf{r} \right) + (T[n_0] + E_{ee}[n_0]) \tag{2.14}$$

The system independent part, i.e. second part of the equation (2.14) is the *Hohenberg-Kohn functional* $F_{HK}[n_0]$. If the form of $F_{HK}[n_0]$ were known, we could have solved the Schrodinger equation for any system, exactly. Due to self interaction, exchange and Coulomb correlation contributions to the electron-electron interactions, makes it harder to find an explicit expression for $F_{HK}[n_0]$.

In summary, ground state electron density of a system uniquely determines the Hamiltonian operator, which characterizes all states of the system, ground and excited. Thus all properties of system are formally determined by the ground state density[5].

**Theorem 2**:"The functional that delivers ground state energy of the system$E[n_0]$, delivers lowest energies if and only if the input density is the ground state density $n_0$"[27]. This is just an articulation of the variational principle which in present case can be expressed as[5]

$$E_0[n_0] \leq E[n'] = T[n'] + E_{ee}[n'] + E_{ext}[n'] \tag{2.15}$$

where $n'$ is the trial density (with appropriate boundary conditions, i e $n'(\mathbf{r}) \geq 0$ and $\int n'(\mathbf{r})d\mathbf{r} = N$ satisfied) corresponding to some external potential $V'_{ext}$. The proof runs as follows, let $\hat{H}'$ be the Hamiltonian associated with the trial density $n'(\mathbf{r})$, with corresponding wave functions $\Psi'$. Consider the wavefunction, associated with the Hamiltonian generated from the external potential $V_{ext}$, as the trial wave function. Then,

$$\langle \Psi' | \hat{H} | \Psi' \rangle = T[n'] + V_{ee}[n'] + \int n'(\mathbf{r}) V_{ext} d\mathbf{r} = E[n'] \geq E_0[n_0] = \langle \Psi_0 | \hat{H} | \Psi_0 \rangle \tag{2.16}$$

which is the desired outcome.

## 2.4 Kohn-Sham Approach

Though Hohenberg and Kohn's theorem tell us the connection between an external potential and ground state density of a system, they don't provide us with a recipe to calculate the same. In 1965, Kohn and Sham have suggested a new approach to calculate the previously unknown universal functionals ($T[n_0]$)). Kohn and Sham replaced the difficult many body interacting problem by a non-interacting reference system build from a set of one electron wave functions having same ground state density as of interacting system, so that the major part of kinetic energy can be computed with good accuracy.[8]
Consider non-interacting reference system with the Hamiltonian containing effective, local potential for each particle $V_s(\mathbf{r_i})$,

$$\hat{H}_s = -\frac{1}{2}\sum_i^N \nabla_i^2 + \sum_i^N V_s(\mathbf{r_i}) \tag{2.17}$$

The Hamiltonian represents non-interacting system so the ground state wave function $\Theta_s$ can be represented by slater determinant of one-electron wave functions $\phi_i$ or Kohn-Sham orbital.[28]. The Kohn-Sham orbital are determined by,

$$\hat{f}^{KS}\ \phi_i\ =\ \epsilon_i\ \phi_i \tag{2.18}$$

with the one electron Kohn-Sham Hamiltonian being

$$\hat{f}^{KS} = -\frac{1}{2}\nabla^2 + V_s(\mathbf{r}) \tag{2.19}$$

The potential $V_s$ must be chosen such that the density obtained by summation of moduli of squared orbitals $\phi_i$, exactly equals the system of our interest.

### 2.4.1 Kohn-Sham Equations

The kinetic energy of non interacting system $T_s$ with the same density of interacting real system is given by

$$T_s = -\frac{1}{2}\sum_{i}^{N}\langle\phi_i|\nabla^2|\phi_i\rangle \tag{2.20}$$

The universal functional in eq(2.14) can be written as,

$$F[n(\mathbf{r})] = T_s[n(\mathbf{r})] + J[n(\mathbf{r})] + E_{xc}[n(\mathbf{r})] \tag{2.21}$$

where $J[n(\mathbf{r})]$ is the classical Coulomb part in $E_{ee}[n(\mathbf{r})]$, i.e

$$J[n(\mathbf{r})] = \frac{1}{2}\int\int\frac{n(\mathbf{r_1})n(\mathbf{r_2})}{r_{12}}d\mathbf{r_1}d\mathbf{r_2} \tag{2.22}$$

and the term $E_{xc}$ includes non-classical contribution to the electron-electron interaction and the difference in the many body and single particle kinetic energy. Its contribution to total energy is small, so it can be approximated. Now the energy functional in eq(2.14) can be rewritten in orbital form as

$$\begin{aligned} E[n] = -\frac{1}{2}\sum_{i}^{N}\langle\phi_i|\nabla^2|\phi_i\rangle + \frac{1}{2}\sum_{i}^{N}\sum_{j}^{N}\int\int|\Phi_i(\mathbf{r_1})|^2\frac{1}{r_{12}}|\Phi_j(\mathbf{r_2})|^2 d\mathbf{r_1}d\mathbf{r_2} \\ -\sum_{i}^{N}\int V_{ext}|\Phi_i(\mathbf{r_1})|^2 d\mathbf{r_1} + E_{xc}[n(\mathbf{r})] \end{aligned} \tag{2.23}$$

The ground state electronic density is the density that minimizes $E[n]$ and hence satisfies the Euler equation

$$\mu = V_{ext} + \frac{\partial F[n]}{\partial n} \tag{2.24}$$

where $\mu$ is the Lagrange multiplier associated with the constraint

$$\int n(\mathbf{r})d\mathbf{r} = N \tag{2.25}$$

substituting eq (2.21) in eq (2.25) gives

$$\mu = V_{eff} + \frac{\partial T_s[n]}{\partial n(\mathbf{r})} \tag{2.26}$$

where the effective potential is defined by

$$V_{eff}(\mathbf{r}) = V(\mathbf{r}) + \frac{\partial J[n]}{\partial n(\mathbf{r})} + \frac{\partial E_{xc}[n]}{\partial n(\mathbf{r})} \tag{2.27}$$

The last term can be identified as *exchange-correlation potential*

$$v_{xc} \;=\; \frac{\partial E_{xc}[n]}{\partial n(\mathbf{r})} \tag{2.28}$$

eq (2.26) with constraint in eq (2.25) is precisely the same equation one obtains on doing density functional theory to a system of non-interacting electrons moving in the external potential $V_s(\mathbf{r}) = V_{eff}(\mathbf{r})$[13]. Therefore for a given $V_{eff}(\mathbf{r})$, one obtains the $n(\mathbf{r})$ that satisfies eq (2.26), by solving N one electron equation

$$\left(-\frac{1}{2}\nabla^2 + V_{eff}(\mathbf{r})\right)\;\phi_i \;=\; \epsilon_i\;\phi_i \tag{2.29}$$

which gives

$$n(\mathbf{r}) = \sum_{i}^{N}\sum_{s} |\Psi_i(\mathbf{r}, s)|^2 \tag{2.30}$$

## 2.5 Exchange-Correlation Functional

Now the problem of finding solution to the system boils down to obtaining a good approximate functional form for $E_{xc}$. The exchange correlation potential is a functional derivative of exchange correlation energy with respect to density eq (2.28). There are different ways in which these can be approximated. The two most commonly used ones are described below.

### 2.5.1 Local Density Approximation (LDA)

LDA are a set of approximations, where the exchange-correlation energy functional depends only on the electronic density at each point $\mathbf{r}$ in space[8][18].

$$E_{xc}^{LDA} \;=\; \int n(\mathbf{r})\epsilon_{xc}[n(\mathbf{r})]d\mathbf{r} \tag{2.31}$$

where $\epsilon_{xc}$ is the exchange-correlation energy per particle for a homogeneous electron gas of charge density $n(r)$. LDA gives exact functional form for a homogeneous electron gas and so for systems with slowly varying density it gives reasonably accurate results. Since LDA depends only on local electronic density it completely ignores any correction to the exchange correlation energy due to the inhomogeneity in density[29]

### 2.5.2 Generalised Gradient Approximation (GGA)

GGA takes information from the local electronic density and the information of surrounding electronic density through gradient of electronic density ($\nabla n(\mathbf{r})$), which takes into account the inhomogeneity of electronic density of the system.

We can write GGA-exchange correlation energy in the following form:

$$E_{xc}^{GGA}[n_\alpha, n_\beta] \;=\; \int f(n_\alpha, n_\beta, \nabla n_\alpha, \nabla n_\beta)d(\mathbf{r}) \tag{2.32}$$

In general GGA improves on LDA for the quantities which are already successfully treated in LDA but GGA gives a more accurate description of the many body electron system than LDA.

## 2.6 Periodic System

Now, the Kohn-Sham orbital $\phi_i$ or the wavefunction can be expanded in terms of a basis set (2.33), so that we can solve the Kohn-Sham equations by diagonalizing an eigenvalue equation as shown in equation(2.34) below.[1]

$$\phi_i(\mathbf{r}) = \sum_{\alpha=1}^{N_b} C_{i\alpha} f(\mathbf{r}) \tag{2.33}$$

$$\sum_{\beta} H_{\alpha\beta} c_{i\beta} \;=\; \epsilon_i C_{i\alpha} \tag{2.34}$$

We can choose set of plane waves as basis set, due to some advantages in calculations for periodic system.

### 2.6.1 Bloch's theorem and Plane wave Basis set

Eigen function $\Psi$ for a periodic system will satisfy Bloch's theorem(3.35).

$$\Psi_{\mathbf{k}}(\mathbf{r}) \;=\; \exp i\mathbf{k}\cdot\mathbf{r}\; U_{\mathbf{k}}(\mathbf{r}) \tag{2.35}$$

where the function $U_{\mathbf{k}}(\mathbf{r})$ possess same periodicity as that of the system. This periodic function is expanded in a discrete set of pane waves as shown below:

$$U_{\mathbf{k}}(\mathbf{r}) = \frac{1}{\Omega}\sum_{\mathbf{G}} C_{\mathbf{k},\mathbf{G}} e^{i\mathbf{G}\cdot\mathbf{r}} \tag{2.36}$$

where $\mathbf{G}$ is the reciprocal lattice vector and $\Omega$ is the unit cell volume. So, we can write an equation for the Bloch wavefunction expanded in a plane wave basis set as in (2.33)

$$\Psi_{\mathbf{k}}(\mathbf{r}) = \frac{1}{\Omega}\sum_{\mathbf{G}} C_{\mathbf{k},\mathbf{G}} e^{i(\mathbf{k}+\mathbf{G})\cdot\mathbf{r}} \tag{2.37}$$

In reality the summation over $\mathbf{G}$ in eq(2.37) contains infinite number of plane waves. But the contribution of plane wave with large values of $\mathbf{G}$ are usually negligible. So one can truncate the expansion at some $|\mathbf{k}+\mathbf{G}|$, which is called the kinetic energy cutoff ($E_{cut}$) and is given by:[19]

$$E_{cut} = \frac{\hbar^2|\mathbf{k}+\mathbf{G}|^2}{2m} = \frac{\hbar^2\mathbf{G}_{cut}^2}{2m} \tag{2.38}$$

After the truncation infinite sum of plane wave in eq (2.37) would become a finite sum

$$\Psi_{\mathbf{k}}(\mathbf{r}) = \frac{1}{\Omega}\sum_{|\mathbf{K}+\mathbf{G}|\leq\mathbf{G}_{cut}} C_{\mathbf{k},\mathbf{G}} e^{i(\mathbf{k}+\mathbf{G})\mathbf{r}} \tag{2.39}$$

### 2.6.2 k-point sampling

For calculating physical quantities like total energy, one would need to do a Brillouin zone (BZ) integration. Periodic boundary conditions allow using a set of discrete kpoints in BZ instead of continuous values for the eigenstate of the Kohn sham equation. Consider a solid system. Since the system has an infinite number of electrons we would require an infinite number of kpoints as well (i.e the density of k points is proportional to the size of the system). Nevertheless, the electronic eigenfunctions of k points that are lying close to each other will be practically identical. So a single k point can be used to represent a set of k points that are lying nearby. So one can divide the BZ into a finite number of pieces for calculating ground state density, total energy etc. With these approximations we can find the electronic states of the system with finite number of k points and finite number of plane waves.

## 2.7 Pseudopotential

Properties of a solid are dictated by the valence electrons of the constituent atoms (than their core electrons). Hence to reduce computational cost, the core electrons are ignored. In the pseudopotential the strong nucleus potential felt by the valence electrons are replaced with a weaker potential screened by the core electrons. In the Kohn-Sham equations, the external potential is replaced with this pseudopotential. Moreover, the core region of the true valence wavefunction, where there are lot of wiggles and requires larger number of plane waves are replaced with a smoother function while the tail part matches the exact wavefunction as shown in Figure:2.1. This modified function is called the pseudo wavefunction. Invention of pseudopotential and pseudo wavefunction with fewer Fourier modes, reduce the size of the plane-wave basis set and make the calculations less expensive. [19]

Norm-conserving and ultrasoft are two of the most widely used pseudopotentials in-plane wave-based electronic structure calculation. Norm-conserving pseudopotential obeys two criteria: 1) true valence electron and pseudo wavefunction must be identical outside a cutoff radius (designated as $r_c$) and 2)the norm of the psuedo wavefunction inside the cutoff radius should match with the true electron wavefunction. The ultrasoft pseudopotential relaxes the norm-conserving condition to decrease the size of the required plane-wave basis set.

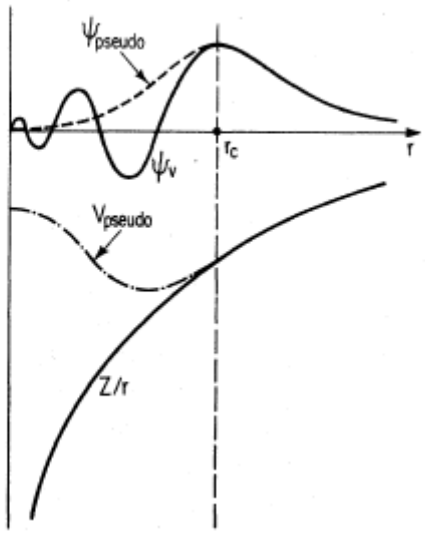


Figure 2.1: Schematic illustration of all-electron (solid lines) and pseudoelectron (dashed lines) potentials and their corresponding wave functions. The radius at which all-electron and pseudoelectron values match is designated as $r_c$ (Reprinted with permission from ref.[19] Copyright 2018, Reviews of Modern Physics)

## 2.8 Self-consistency cycle

The effective potential in the Kohn-Sham equation eq (2.29) depends on density which is an unknown quantity. So one needs to solve the equation using an iterative procedure or self consistently to find the solution. The same is schematically shown below

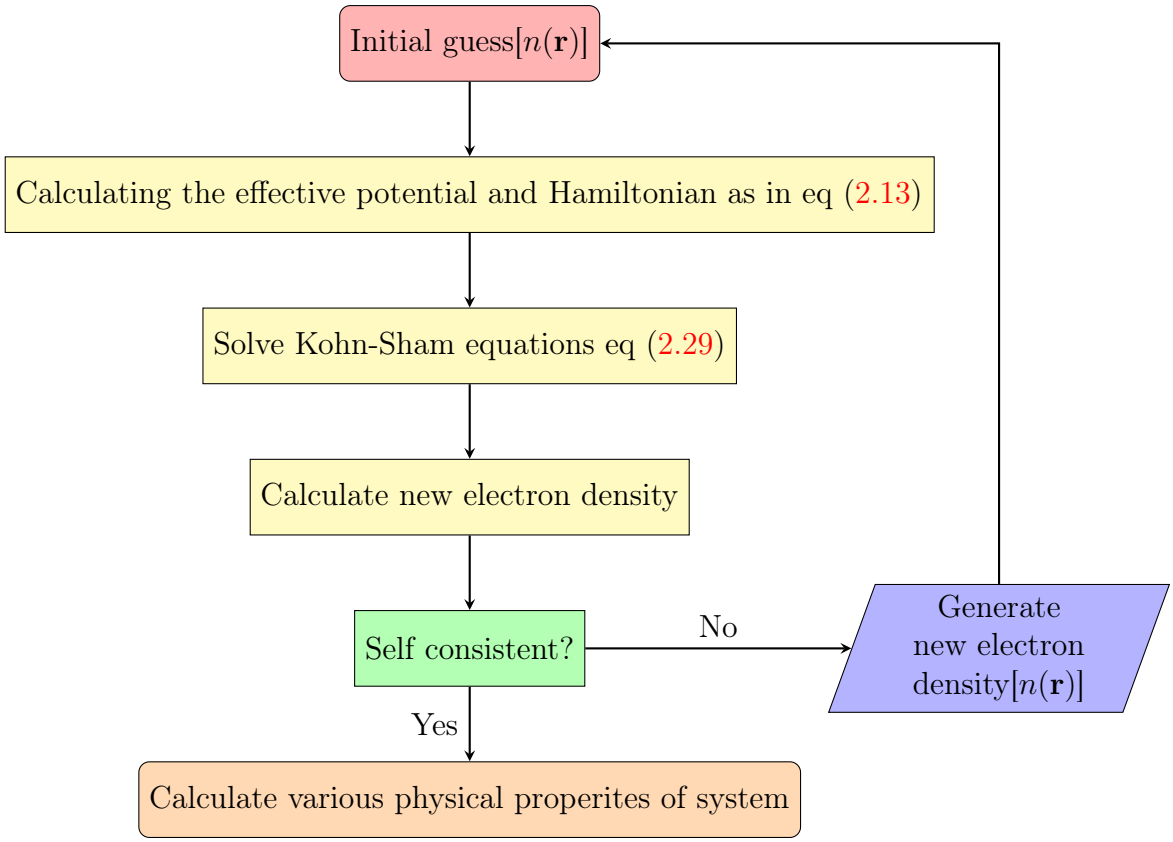


## 2.9 Band Unfolding

### 2.9.1 Supercell

Bloch's theorem cannot be applied to a system containing a single defect because the periodicity is broken. Continuous plane wave basis would be needed for such calculation, hence infinite number of plane waves are required for such calculation. So we use a periodic supercell (SC) construction to study the effect of defect (figure **??**). A supercell is mathematical construction acheived by repeating a primitive cell(PC) unit along one or more spatial directions. Size of the supercell can be determined according to the defect concentration. [19]

### 2.9.2 Unfolding the band structure

Even though it is possible to get energy bands ($E(\vec{K})$) for an SC calculation (and it contains same amount of the information as in PC description), its interpretation is difficult due to its complex nature. Because increasing the size of the unit cell in real space will decrease the size of the unit cell in reciprocal space and thus increasing the number of bands in k space or folding of bands in k space. So extracting the energy diagram ($E(\vec{k})$) for PC is more convenient.

As described in Ref. [23], there is a computational procedure with which one can get effective band structure (EBS) from SC energy eigenvalues. The SC eigenvalues

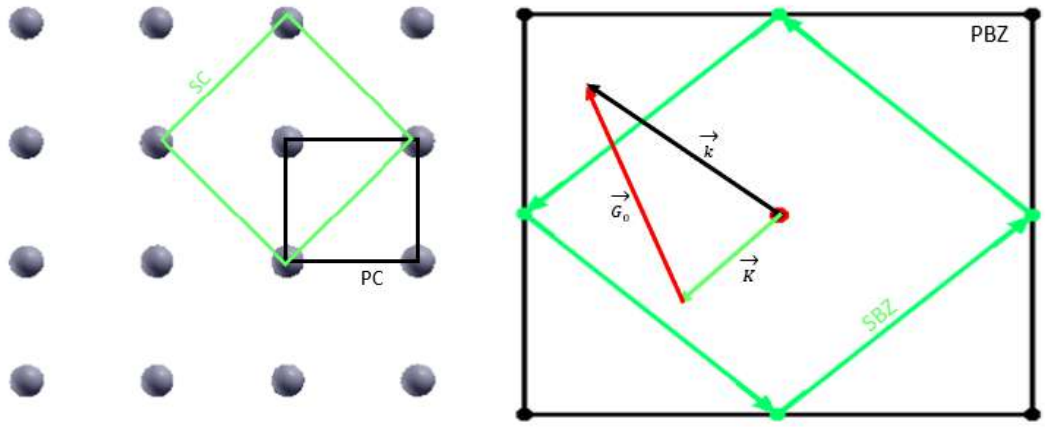


(a) (b)

Figure 2.2: a) Primitive cell, supercell b) Brillouin zone(PBZ and SBZ)

are obtained by explicitly diagonalizing the single-particle Kohn-Sham equation for super cell.

One can describe reciprocal space by the wave vector either from primitive Brillouin zone ($\vec{k}$) or supercell Brillouin zone ($\vec{K}$) and the corresponding energy dispersion can be easily obtained $E(\vec{k})$ and $E(\vec{K})$. Then the unfolding procedure can be used to reconstruct $E(\vec{k})$ from $E(\vec{K})$ (Figure:2.2)

Consider a fictitious ordered periodic system(2D) (Fig. 2.2). If one can find a reciprocal lattice vector $G_0$ , which satisfies eq(2.40), then the wave vector $\vec{k}$ (in primitive BZ) can be folded into into a wavevector $\vec{K}$(in Supercell BZ),(2.2b) by

$$\vec{K} = \vec{k} - \vec{G}_0 \tag{2.40}$$

Similarly, wave vector $\vec{K}$ can be unfolded into $\vec{k_i}$ in pbz,if

$$\vec{k_i} = \vec{K} + \vec{G}_i, \quad i = 1, \ldots, N_{\vec{k}} \tag{2.41}$$

where $N_{\vec{k}}$ is the number of different ways one can unfold $\vec{K}$ and is equal to the determinant of the transformation matrix which transforms PC to SC. By solving the associated Schrodinger equations, one can get the energy eigenstates $|\vec{k}n\rangle$ and $|\vec{K}m\rangle$ for both PC and SC respectively (with n, m being band indices). The geometric relations of band folding and unfolding of wave vector, allows us to write any SC eigenvector $|\vec{K}m\rangle$ as a linear combination of PC Bloch state $|\vec{k_i}n\rangle$ , $i = 1, \ldots, N_{\vec{k}}$.

$$|\vec{K}m\rangle = \sum_{i=1}^{N_{\vec{k}}} \sum_{n} F(\vec{k}_i, n; \vec{K}, m) \, |\vec{k}_i n\rangle \tag{2.42}$$

By projecting $|\vec{K}m\rangle$ on all possible PC eigenvector $|\vec{k_i}n\rangle$ of fixed $k_i$, calculating the spectral weight, one obtains

$$P_{\vec{K}m}(\vec{k}_i) = \sum_n |\langle \vec{K}, m|\vec{k}_i, n\rangle|^2 \tag{2.43}$$

from $P_{\vec{k}m}(\vec{k}_i)$. It is straight forward to derive the spectral function (SF) of continuous variable $E$.

$$A(\vec{k}_i, E) = \sum_m P_{\vec{K}m}(\vec{k}_i)\delta(E_m - E) \tag{2.44}$$

Equation in (2.44) can be directly used to obtain $E(\vec{k})$ from $E(\vec{K})$

## 2.10 Boltzmann Transport properties

Boltzmann theory is a useful concept for understanding the transport properties of real materials. The electric current $j_i$, under the influence of an electric field $E$ and temperature gradient $\nabla T$ can be expressed in terms of conductivity tensors $(\sigma_{i,j})$.([11])

$$j_i = \sigma_{ij}E_j + v_{ij}\nabla_j T \tag{2.45}$$

The conductivity tensor can be written in terms of group velocity and mass tensor as,

$$\sigma_{\alpha\beta}(i, \vec{k}) = e^2\tau_{i,\vec{k}}v_\alpha(i, \vec{k})v_\beta(i, \vec{k}) \tag{2.46}$$

where the group velocity is

$$v_\alpha(i, \vec{k}) = \frac{1}{\hbar}\frac{\partial\epsilon_{i,\vec{k}}}{\partial k_\alpha} \tag{2.47}$$

and the mass tensor is

$$M^{-1}_{\beta\alpha}(i, \vec{k}) = \frac{1}{\hbar^2}\frac{\partial^2\epsilon_{i,\vec{k}}}{\partial k_\beta \partial k_\alpha} \tag{2.48}$$

We will approximate the relaxation time to be independent of the electronic state and temperature and hence a constant. Conductivity tensors in terms of energy can be obtained by projecting density of states with the conductivity tensor as given in the equation below:

$$\sigma_{\alpha\beta}(\epsilon) = \frac{1}{N}\sum_{i,\vec{k}} \sigma_{\alpha\beta}(i, \vec{k})\frac{\delta(\epsilon - \epsilon_{i,\vec{K}})}{d\epsilon} \tag{2.49}$$

This is the transport distribution function; now the major transport tensors in eq (2.45) can be calculated as:

$$\sigma_{\alpha,\beta}(T;\mu) = \frac{1}{\Omega}\int \sigma_{\alpha,\beta}(\epsilon)\left[\frac{-\partial f_\mu(T;\epsilon)}{\partial\epsilon}\right]d\epsilon \tag{2.50}$$

$$v_{\alpha,\beta}(T;\mu) = \frac{1}{eT\Omega}\sigma_{\alpha,\beta}(\epsilon)(\epsilon - \mu)\left[\frac{-\partial f_\mu(T;\epsilon)}{\partial\epsilon}\right]d\epsilon \tag{2.51}$$

The Seebeck coefficient can be calculated as:

$$S_{i,j} = E_i(\nabla_j T)^{-1} = (\sigma^{-1})_{\alpha,i}v_{\alpha,j} \tag{2.52}$$

Thermal conductivity due to electron, $k^0$ can be calculated as:

$$k^0_{\alpha,\beta}(T;\mu) = \frac{1}{e^2 T\Omega}\sigma_{\alpha,\beta}(\epsilon)(\epsilon-\mu)^2\left[\frac{-\partial f_\mu(T;\epsilon)}{\partial\epsilon}\right]d\epsilon \tag{2.53}$$

# Chapter 3

# Results and Discussion

This chapter contains the results of the study of the structure, electronic structure and the transport properties of both $\alpha$-$BaCu_2S_2$ and $\beta$-$BaCu_2S_2$ phase with different dopants for improving thermoelectric performance.

## 3.1 Computational Details

We have used the Quantum Espresso[3] software for electronic structure calculations and geometry optimization, which is based on Density Functional Theory, plane-wave basis sets and pseudopotentials. Ultrasoft pseudopotentials have been used for including the interaction between ionic cores and valence electrons. Following are the valence electron configuration of the atoms in the calculation: Ba-$5s^25p^66s^2$, Cu-$3d^{10}4s^1$, S-$3s^23p^4$, Al-$3s^23p^1$, Ga-$4s^23d^{10}3p^1$, In-$5s^24d^{10}5p^1$, Tl-$6s^25d^{10}6p^1$, As-$4s^24p^3$, Sb-$4d^{10}5s^25p^1$. The electron-electron exchange correlation functional is described by the Perdew–Burke–Ernzerhof (PBE) parametrization of GGA[21]. A kinetic energy cutoff of 45 Ry has been used for the wavefunction and a kinetic energy cutoff of 450 Ry has been used for the charge density. Brillouin zone integrations are done by using a Monkhorst-Pack $k$-grid of $12 \times 5 \times 5$ and $12 \times 12 \times 4$ for the orthorhombic and tetragonal phase respectively. Total energy convergence of $10^{-6}$ eV has been adopted for the calculation. The orthorhombic phase contains 20 atoms per unit cell and the tetragonal one contains 10 atoms per unit cell.

For the calculation with dopants, $2 \times 2 \times 1$ and $2 \times 1 \times 1$ supercells, with 40 atoms each, have been used for the tetragonal and orthorhombic phases respectively. Accordingly, $k$-grids of $6 \times 5 \times 5$ (orthorhombic supercell),$6 \times 6 \times 4$ (tetragonal supercell) have been used for BZ integration. The dopants we tried are Al, In, Ga, Tl, As and Sb. We did not use any smearing for calculations of the undoped system. For the ones with dopants, to speed up the convergence, we have used Marzari-Vanderbilt[14] smearing with a smearing width of 0.003 Ry.

Boltzmann Semi-classical transport equation as implemented in BoltzTraP[11] software code has been used to extract the electronic transport coefficients. The software uses Fourier expansion to interpolate bands for calculation.The convergence of transport coefficeints have been acheived by using dense k-mesh of $48 \times 48 \times 16$ and $48 \times 20 \times 20$ for Tetragonal and Orthrhombic respectively, with a Fourier interpolation factor of 15.

Table 3.1: Comparison of lattice parameters of $BaCu_2S_2$.

| lattice parameter | calculated | Experiment(lit) | Theoretical(lit) |
|---|---|---|---|
| orthorhombic phase | | | |
| a(Å) | 4.027 | 4.055[15] | 4.051[22] |
| b(Å) | 9.385 | 9.280[15] | 9.281[22] |
| c(Å) | 10.32 | 10.39[15] | 10.41[22] |
| Tetragonal Phase | | | |
| a(Å)=b(Å) | 3.89 | 3.92[6] | 3.92[10] |
| c(Å) | 12.60 | 12.66[6] | 12.62[10] |

## 3.2 Structure

$BaCu_2S_2$ is a ternary copper chalcogenide, which is relatively unexplored material, while another member of this family, $BaCu_2Se_2$, is known to exhibit excellent thermoelectric performance. $BaCu_2S_2$ exist in two configurations, a low temperature phase that have an orthrohombic structure ($\alpha$-$BaCu_2S_2$) and a high temperature-tetragonal one ($\beta$-$BaCu_2S_2$). Both $\alpha$-$BaCu_2S_2$ (with pnma space group) and $\beta$-$BaCu_2S_2$ (with I4/mmm Space group) are intrinsic semiconductors, with $\alpha$-$BaCu_2S_2$ having good thermopower[15](50-500 $\mu V/K$) and $\beta$-$BaCu_2S_2$ having low thermal(0.86 $Wm^{-1}K^{-1}$ at room temperature) and electric conductivity. The tetragonal phase is relatively more explored than the orthorhombic one.

From our calculations the $\alpha$-phase turned out to be 0.12 ev/formula unit more stable than the $\beta$ one. The optimized lattice parameters for both the phases, obtained from our calculations are in good agreement with the reported values (Table:3.1). The orthorhombic structure contains 2 different Wyckoff position for both the the sulphur (S6,S7-number does not have any significance other than identification) and copper (Cu10,Cu11) (Figure:3.1 a). Orthorhombic structure contains a tetrahedrally bonded copper and sulphur network(Figure:3.1 b) with barium occupying in between. The tetrahedra is distorted and contains 2 pairs of Cu-S bonds. The Cu-S bond length depends on identity of both the element. A tetrahedra around Cu10 contains a pair of bonds of length, 2.47 Å each with S7 and another pair each having a length of 2.41 Å with S6. In contrast, for Cu11, there are three types of Cu-S bond lengths: two Cu-S bonds, each of 2.38 Å , with S6, one Cu-S bond of length 2.49 Å with S6 and a third one with S7 of length 2.39 Å. The tetragonal crystal has a layered appearance along the $c$-axis, with $Cu_2S_2$ layers are sandwiched between Ba layers (Figure:3.1 c). Each $Cu_2S_2$ layer is made up of edge-sharing $CuS_4$ tetrahedra, with a Cu-S bond length of 2.42 (2.41[10])Å.

Band structure and the density of states for each phase are shown in Figure:3.2. Both $\alpha$ and $\beta$ phase are semiconductors with a direct band gap of 0.80 eV and 1.10 eV respectively, occurring at $\Gamma$ point of the BZ. The experimentally reported value of band gap is 1.75 eV for the tetragonal phase, which is severely underestimated in our calculation. This is expected with the use of an approximate exchange correlation functional([7]). To the best of my knowledge, I have not come across any experimental report on the band gap of the orthorhombic phase.

In both the phases the primary (VB near bandgap) and secondary (band be-

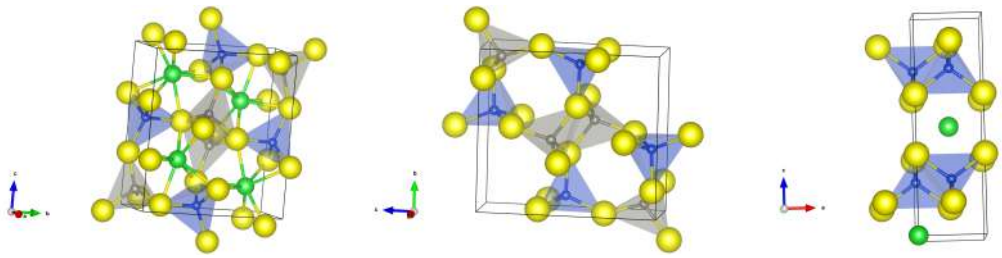

(a) (b) (c)

Figure 3.1: a: Structure of the orthorhombic phase. b: The Cu-S tetrahedral network. c: Structure of the tetragonal phase.(For orthrhombic phase grey Cu-Cu11, blue Cu-Cu10)(Ba-green, S-yellow Ionic radius have been considered)

low -3 eV in both the phases) valences arise from hybridization of copper (3d) and sulphur (3p) orbitals. The primary and secondary valence band (not shown in 3.2) corresponds to antibonding and bonding orbitals respectively. The antibonding nature of the valence band is confirmed by plotting the integrated local density of states(ILDOS) near the band edge, where the charge density of the orbital is concentrated near induvidual atom than in-between the atoms. As expected Sulphur, a more electronegative atom than copper have a larger contribution to the bonding orbital than Cu. Major contribution to the conduction band is from Ba 5d orbital. In both the phases two electron from a Ba atom goes into the antibonding orbital of $Cu_2S_2$(Figure:3.2c,d) which makes Ba-$Cu_2S_2$ interaction ionic in nature. In contrast, Cu and S in $Cu_2S_2$ form covalent bonds. In the tetragonal phase, Cu-Cu also has the bonding and antibonding nature in VB as Cu-S interaction[7]. Whereas the Ba-S interaction is always bonding in nature in VB. So the Ba sheets between $Cu_2S_2$ layer have an important role in the structural stability of the $\beta$-$BaCu_2S_2$.

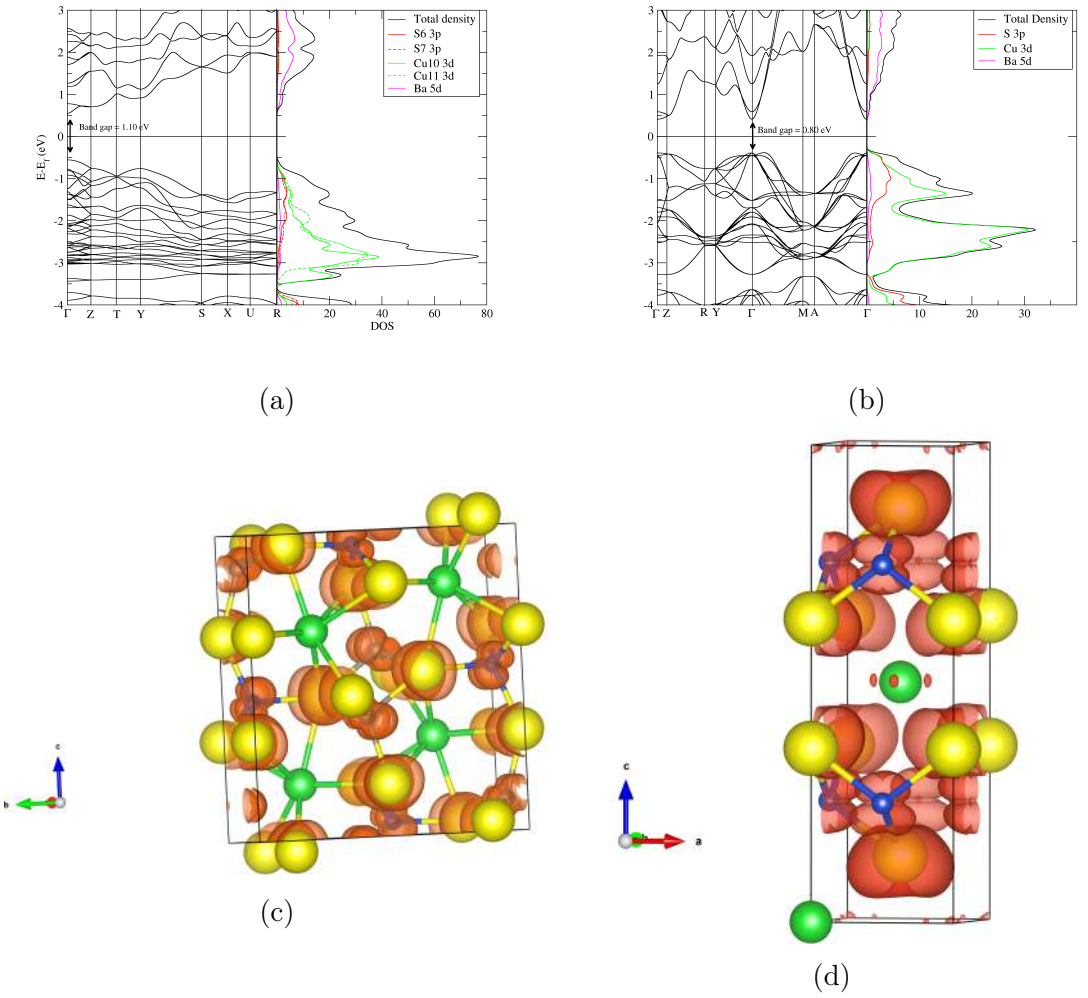


(a) (b)

(c) (d)

Figure 3.2: Band structure($left$) and projected density of states($right$) for a)$\alpha$$BaCu_2S_2$ b)$\beta$−-$BaCu_2S_2$ and integrated local density plots near VB edge for c) orthorhombic phase (from VBM to 0.19 eV below VBM) and d) tetragonal phase (from VBM to 0.20 eV deep into VBM).

The mobility of charge carriers depend upon their effective masses ($m^*$), which are the curvature of the band structure. Effective masses have been calculated by invoking parabolic band approximation at Γ point for both the conduction band minimum (CBM) and the valence band maximum (VBM). $m^*$ for CBM (VBM) provides information about the effective mass of electrons (holes). The effective masses for the charge carriers along two high symmetry directions are listed in Table:3.2). We find that generally the holes are heavier than electrons in both the phases. In the orthorhombic phase, the holes along $\Gamma \rightarrow Y$ and $\Gamma \rightarrow Z$ have significantly larger effective mass than the electrons, while the holes and electrons have comparable effective mass along $\Gamma \rightarrow X$ direction. Moreover, the hole effective masses are also significantly different along different BZ directions highlighting the anisotropy in the structure. In the tetragonal phase, electrons are lighter than the holes in general. Along $\Gamma \rightarrow M$, hole is about 1.5 times heavier than the electron

while along $\Gamma \rightarrow R$ and $\Gamma \rightarrow Z$ the holes are about six and four times heavier than electrons. Moreover, both electrons and holes have very highe effective masses along $\Gamma \rightarrow Z$ directions due to the layered structure perpendicular to the z-axis in real space, i.e the anisotropy in the structure.

Table 3.2: Effective masses (in units of $m_e$) of holes and electrons in $BaCu_2S_2$ as obtained from the parabolic band approximation.

| Direction | Holes | Electrons |
|---|---|---|
| $\alpha$-phase | | |
| Γ-X | 0.28 | 0.22 |
| Γ-Y | 1.46 | 0.48 |
| Γ-Z | 1.64 | 0.28 |
| $\beta$-phase | | |
| Γ-M | 0.27 | 0.17 |
| Γ-R | 1.66 | 0.27 |
| Γ-Z | 8.63(4.91[7]) | 2.21(2.20[7]) |

For both the phases Tetragonal and Orthorhombic, the major contribution to conduction band is from Ba-$d$ orbital. But intuitively we expect the contribution from Ba-$s$ orbital, since that is the valence most orbital. But this may be due to the shift in Ba-$s$ energy level, up in energy than d-orbital upon forming crystal. Isolated Ba-$s$ orbital is very delocalised in nature, so the narrow spacing in solid pushes the Ba-s states high in energy[10]. Both the phases are experimentally reported to be p-type material, i.e. dominant carriers are holes, which is originating from the copper vacancies[15]. The p type nature in tetragonal phase is predicted, due to low ionisation energy and small electron affinity as described in [10].

## 3.3 Doping

Following are the dopants we tried in both phases of $BaCu_2S_2$ to identify resonant dopants: Aluminium (Al), Gallium (Ga), Indium (In), Thallium (Tl) (all are Group 13 elements) and Arsenic(As) and Antimony (Sb) from Group 15. One atom in the supercell is replaced with dopant from one parent formula unit out of 8 formula units. So the doping concentration is 12.5% formula unit.

### 3.3.1 Structure and Formation Energy

Formation energy for a dopant is the energy required to substitute a parent atom. Lower formation energy means it is easier to get that particular substitution done. We have substituted every atomic species with all the dopants and calculated the formation energy($E^f$), which is given as (eq. 3.1)

$$E^f = E_{tot} - E_{pristine} - E_R + E_X \tag{3.1}$$

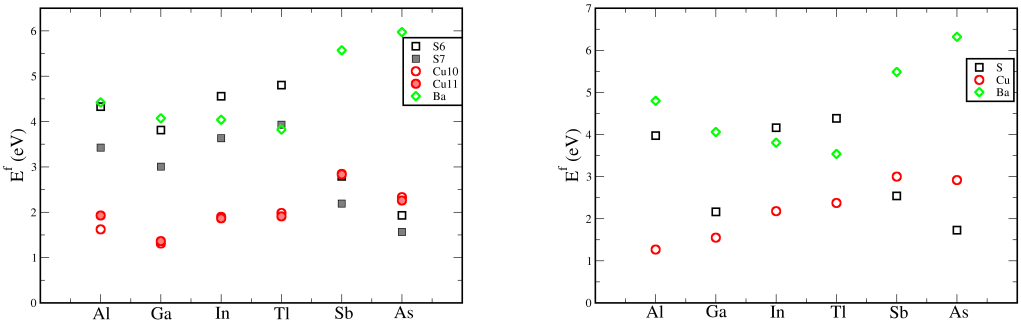


(a) (b)

Figure 3.3: Formation energy of various doping in a) $\alpha$-$BaCu_2S_2$ b) $\beta$-$BaCu_2S_2$

where $E_{tot}$ and $E_{pristine}$ are the total energies of doped and parent supercell respectively and $E_R, E_X$ are the bulk phase energy of dopant and the atom that get replaced respectively.

As is evident from Figure:3.3, for both the phases, Group 13 elements prefer to occupy the Cu site while As and Sb prefer to occupy the S site. Moreover, in the $\alpha$-$BaCu_2S_2$ replacing Cu10 with Ga is the most favoured doping. For the other Group 13 elements the formation energies for occupying Cu10 and Cu11 sites in the $\alpha$ are comparable.

The dopants introduce significant distortions in the dopant-S or dopant-Cu bond lengths. For example when the group 13 elements occupy Cu10 site, the Cu10-S7/S6 bond lengths are elongated. Moreover for these cases the two dopant-S7 bonds that were equal in the parent compound still remains equal, though significantly elongated. These bond lengths vary between 2.66-2.80 Å with Al having a value of 2.66 Å and Tl-S7 bond length being 2.80 Å. The degeneracy of the Cu10-S6 bond lengths are broken and now we have two dopant-S6 bonds. Here also the bond length increases as one goes down the periodic table. At the Cu11 sites, when the dopants are Ga, In and Tl, the bond lengths are significantly elongated and varies between 2.60 and 2.89 Å. In contrast, the Al-S6 and Al-S7 bond lengths are shortened and lies between 2.27 and 2.33 Å. However, in this case also the dopant-S bond lengths increase as we go down the periodic table. In contrast when Sb occupies S7 sites the Sb-Cu bond lengths are either similar to that of Cu-S or are slightly elongated. For As, all the As-Cu bond lengths are larger compared to the Cu-S bond lengths.

For the tetragonal phase, only when Al occupies the Cu site the Al-S bond lengths are shortened to 2.33 Å. In the case of Ga/In/Tl occupying the bond lengths increase and comparable to those observed for the orthorhombic phase. The Sb/As-Cu bond lengths compared to Cu-S bond lengths in tetragonal phase are similar to those observed in the orthorhombic phase.

### 3.3.2 Effect of doping on the electronic structure

To understand the effect of doping on the electronic structure of the parent compounds, we have plotted the total density of states of the doped system and their projections on the atomic orbitals of the dopant atoms, band structure for each configuration unfolded onto the primitive unit cell Brillouin zone and the integrated local density of states (ILDOS) corresponding to the peaks in the DOS arising from the dopant states.

## Aluminium

In orthorhombic phase, doping of Aluminium at Cu10 site give rise to two defect states. One empty state at the bottom of the conduction band(Figure:3.4(a)) due to the hybridization of the $p_x$ orbital of Aluminium and $p$ orbitals of surrounding sulphurs as is evident from the projected DOS plots (Figure:3.4(a)). The second occupied state at the the gap, but closer to the conduction band is from Al $s$. Additionally, the py and pz states of Al hybridizes with those of the S atoms of the host lattice. When the Cu atom is extracted from the lattice, it leaves behind a hole. On adding Al it contributes 3 extra electron, of which one compensates the hole. The other 2 electrons also reside in the Cu-S network. However, due to the nature of hybridization of the Al orbitals with those of S results in completely filled bands. This is in contrast with the conventional electron doping where the conduction band is usually partially occupied.

On replacing the Cu11 atom with Al, we find the dopant states hybridize strongly with that of the parent compound resulting in more delocalized state. As a consequence, we observe partially filled conduction band that makes the system metallic (Figure:3.4(b)). The stronger hybridization can be justified with smaller average Al (Cu11)-S bond length of 2.31 Å (Al (Cu10)-S has on an average 2.58 Å of bond length).

Al in tetragonal phase did not show any desired features of resonant doping. The behaviour of Al in tetragonal was similar to that of Al (Cu11)-case(Figure:3.5(a)). Both orbitals (s and p) were greatly delocalized, with Al acting merely as an electron donor.

Al doping at Cu10 site only could produce a distinct defect site in the CB from the $p_x$ orbital of Al. Which can be undertood from the favoured position of $p_x$ orbital to hybridize with p orbitals of neighbouring S atoms.

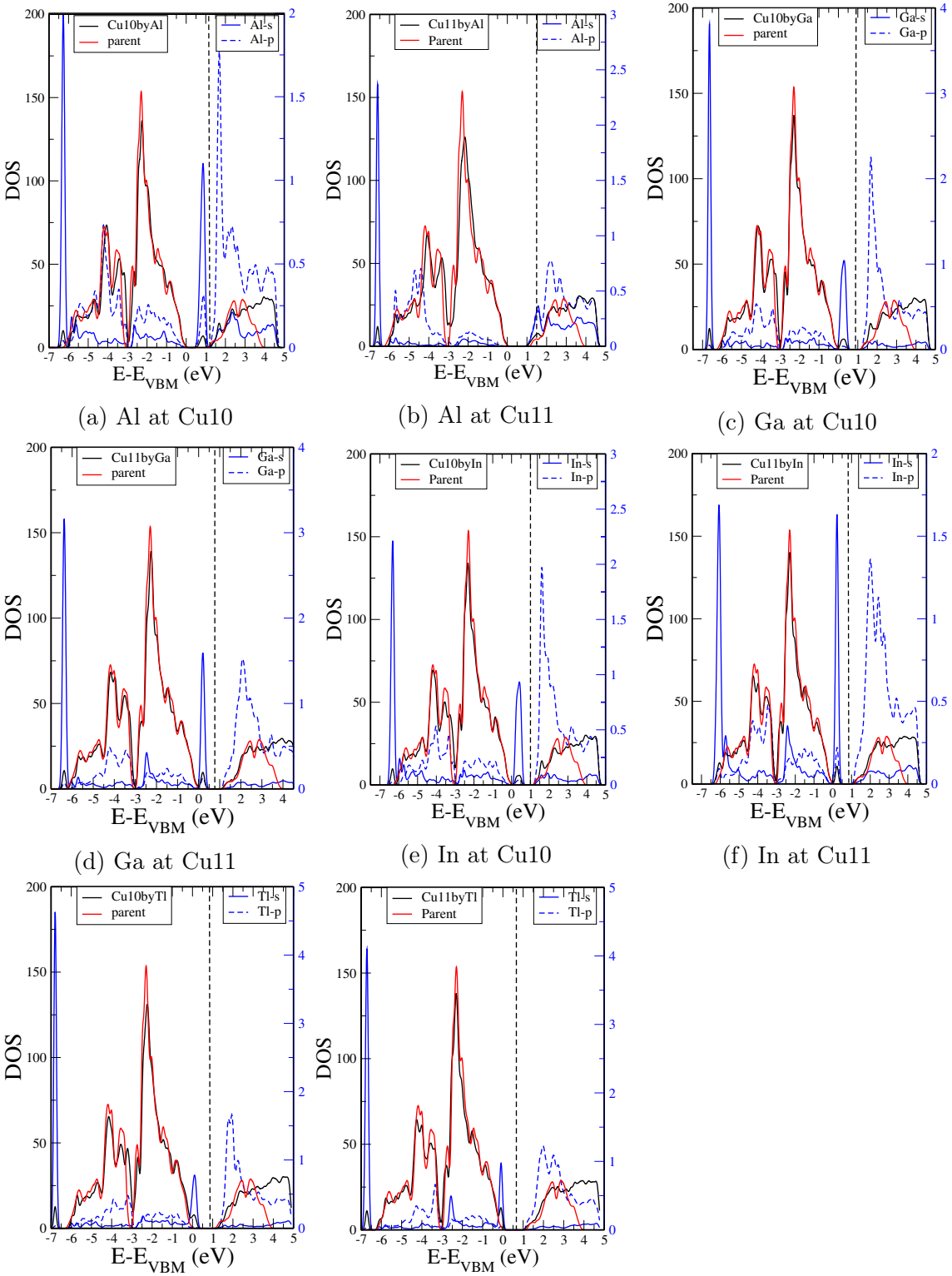


(a) Al at Cu10 (b) Al at Cu11 (c) Ga at Cu10

(d) Ga at Cu11 (e) In at Cu10 (f) In at Cu11

(g) Tl at Cu10 (h) Tl at Cu11

Figure 3.4: Group 13 Doping in orthorhombic $BaCu_2S_2$

## Gallium

Doping of Ga at Cu10 site of orthrhombic phase created two defect states (Figure:3.4(c)). One at the band gap due to the hybridization of Ga-s orbital with p orbitals of surrounding host S atoms and other state at the bottom of conduction band from the hybridization $p_x$ orbital of Ga with the p orbitals of S atoms. The $p_y$, $p_z$ orbital hybridizes strongly with the parent compound to give a more delocalized state in conduction band and deep valence band. This different behaviour of p-orbitals in Ga is related to favourable position of $p_x$ orbital of Ga for overlapping with the S orbitals.

While doping of Ga at Cu11 site created one distinct defect state due to the hybridization of Ga-s with the p-orbital of Ga and of neighbouring S atoms in the band gap, but with higher intensity than the state due to Ga-doping at Cu10 (Figure:3.4(d). The position of this new state remained same. Here the strong hybridization among p orbitals of Ga, resulted in a very delocalized state in the CB. This is in contrast with the Al case, where both s and p orbitals hybridizes.

Ga doping at Cu in tetragonal phase has created a defect state in the band gap from the hybridization of Ga-s orbital with the p orbital selected neighbouring S atoms. The strong hybridization of mixed $p_x, p_y$ with $p_z$ gave a very delocalized state in the CB (Figure:3.5(b)). For all the cases of Ga doping the defect states below Fermi level was enough accommodate the extra 2 electron from Ga (after compensating one electron for the hole created by copper), resulting in filled bands.

## Indium

Behaviour of Indium was similar to Ga. In doping at Cu10 site gave rise to two defect states one in the gap (little more farther from VB than for Ga at Cu10 site) due to the In-s hybridization with p-orbital of sulphur atoms. The second state at the bottom of the conduction band was due to the hybridization of $p_x$ orbital with p orbital of neigbouring sulfur, again Cu10 site favoured this hybridization(Figure:3.4(e)).

Replacing Cu11 by In, gave rise to a distinct state in the band gap but close to VB due to hybridization of In-s with p orbitals of surrounding host S atoms. Improved the intensity of the peak than that of the In doping at Cu10 site. The strong hybridization among In p orbitals and with surrounding S orbitals resulted in a very delocalized state in the CB. Indium doping at Cu10 and Cu11 sites created new states in VB which is enough to accommodate the extra two electrons of Ga in the Cu-S network(Figure:3.4(f).

In doping at Cu of Tetragonal Phase also created a distinct defect state in the middle of the band gap due to hybridization of In-s with p orbitals of selected sorrounding S atoms. The strong hybridization of p-orbitals of In resulted in a very delocalized state in the CB. These two state together made continuum of states. Which gave system a metallic behaviour(Figure:3.5(c).

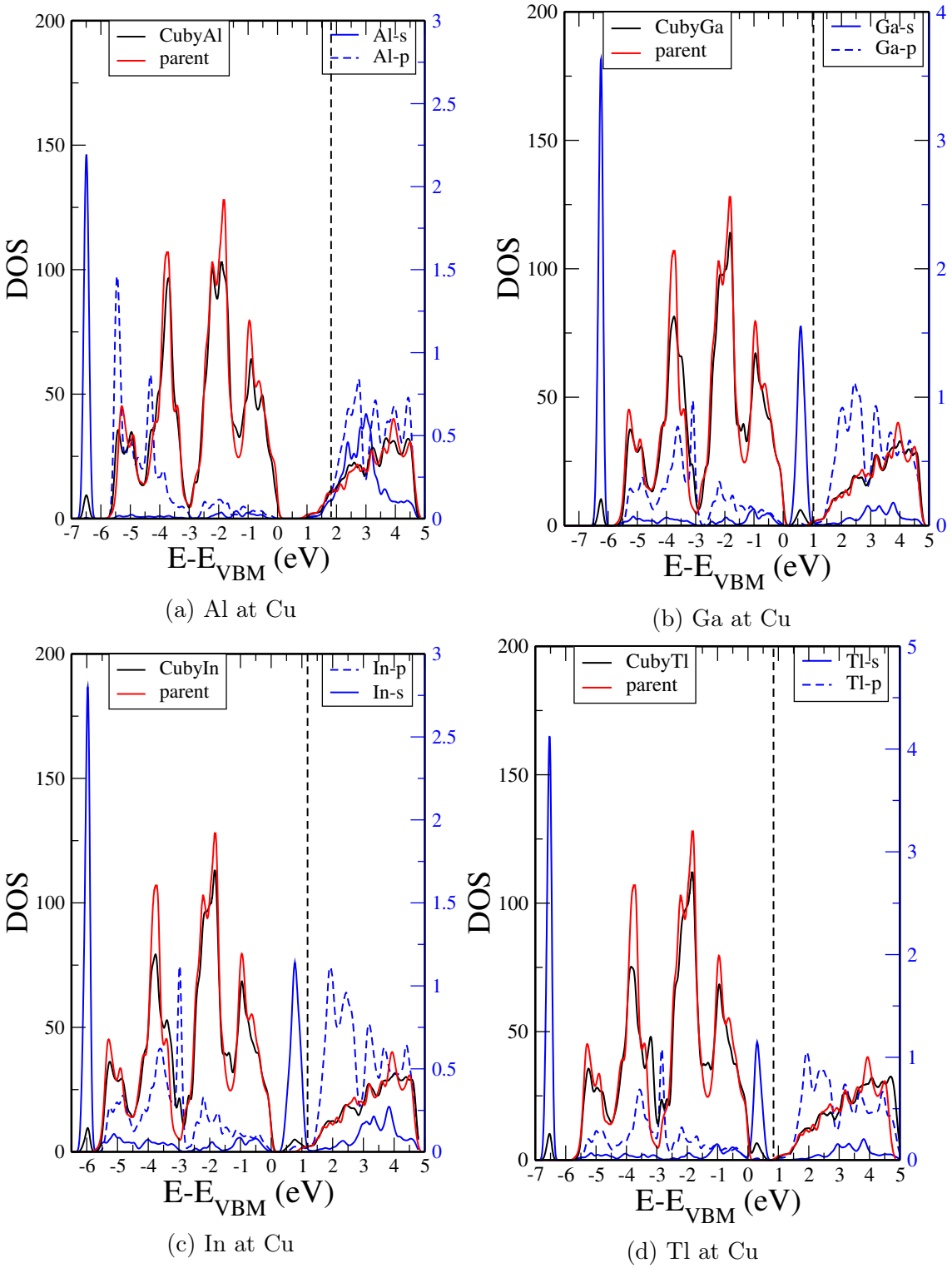


(a) Al at Cu

(b) Ga at Cu

(c) In at Cu

(d) Tl at Cu

Figure 3.5: Group 13 Doping in tetragonal $BaCu_2S_2$

## Thallium

Doping of Tl at Cu10 site created 2 distinct defect state, one at the edge of the VB (unlike the other dopants) due to hybridization of Tl-s orbital with p orbitals

of neighbouring host sulphur atoms and the other state at the bottom of the conduction band from mixing of Tl-$p_x$ orbital and surrounding S-p orbitals. While the $p_z, p_y$ orbital hybridize strongly and gave rise to very delocalized state in the CB(Figure:3.4(g)).

Tl doping at Cu11 site has also created a defect state in VB edge due to hybridization of Tl-s with p orbitals of surrounding S in varying degree. The defect state is narrower from the previous case. Strong hybridization of Tl-p orbitals created a very delocalized band in the CB(Figure:3.4(h)).

Tl doping at Cu site of the Tetragonal phase has also created a defect state in the VB edge with Tl-s and S-p orbitals hybridization. A very delocalized state from the Tl-p orbitals resulted in reduction of the band gap. All the 3 cases of Tl doping, Tl with 3 electrons substituted copper with 1 electron. Unlike in the conventional doping the extra 2 electron after compensating the 1 hole got accommodated in the new VB defect states(Figure:3.5(d)).

For all the doping at Cu11 site have got large R-S (R=Al,Ga,In,Tl) bond length variation is observed than that in Cu10 site, this is due to the presence of defect state in the large range of VB.

## Arsenic

As doping at S7 site is the most stable configuration. As doping at S7 site results in a defect state at the top the VB, due to a weak hybridization with As-$p_y$ orbitals with localized d($d_{z^2}$) orbitals of neighbouring copper atoms. While the $p_x, p_z$ orbitals of As hybridize with other d orbitals of Cu and contribute to the deep VB. The As-s orbitals hybridize with the host Cu-s orbital results in a delocalized state in the CB. Doping with As at S site results in a single hole making the VB partially occupied resulting in metallic behaviour (Figure:3.6a).

As doping at S site of the Tetragonal phase, showed magnetic property with an absolute magnetization of 0.34 $\mu_B$/cell. Here also we observe hybridization between As-$p$ and Cu-$d$ states (Figure:3.6(b)).

## Antimony

Similar to As doping, Sb replaces S7 in the most stable configuration in orthorhombic phase. As doping gave rise to states with sharp peaks at the edge of the VB (near Fermi level) and at the bottom of the valence band. The first is due to hybridization of Sb-$p_y$ orbital with $d_{z^2}$ of surrounding Cu atoms. Second defect state was deep in the VB from hybridization of $p_x, p_z$ orbital of Sb with the other d orbitals of host Cu atoms. While Sb-s hybridizes with Cu-s to form a delocalised state in the conduction band(Figure:3.6(c)).

Sb doping at S site in tetragonal phase showed magnetic property with a very small magnetic moment of 0.08 $\mu_B$/cell. Similar to the previous case As gave rise to two defect state with the corresponding hybridization as mentioned above.

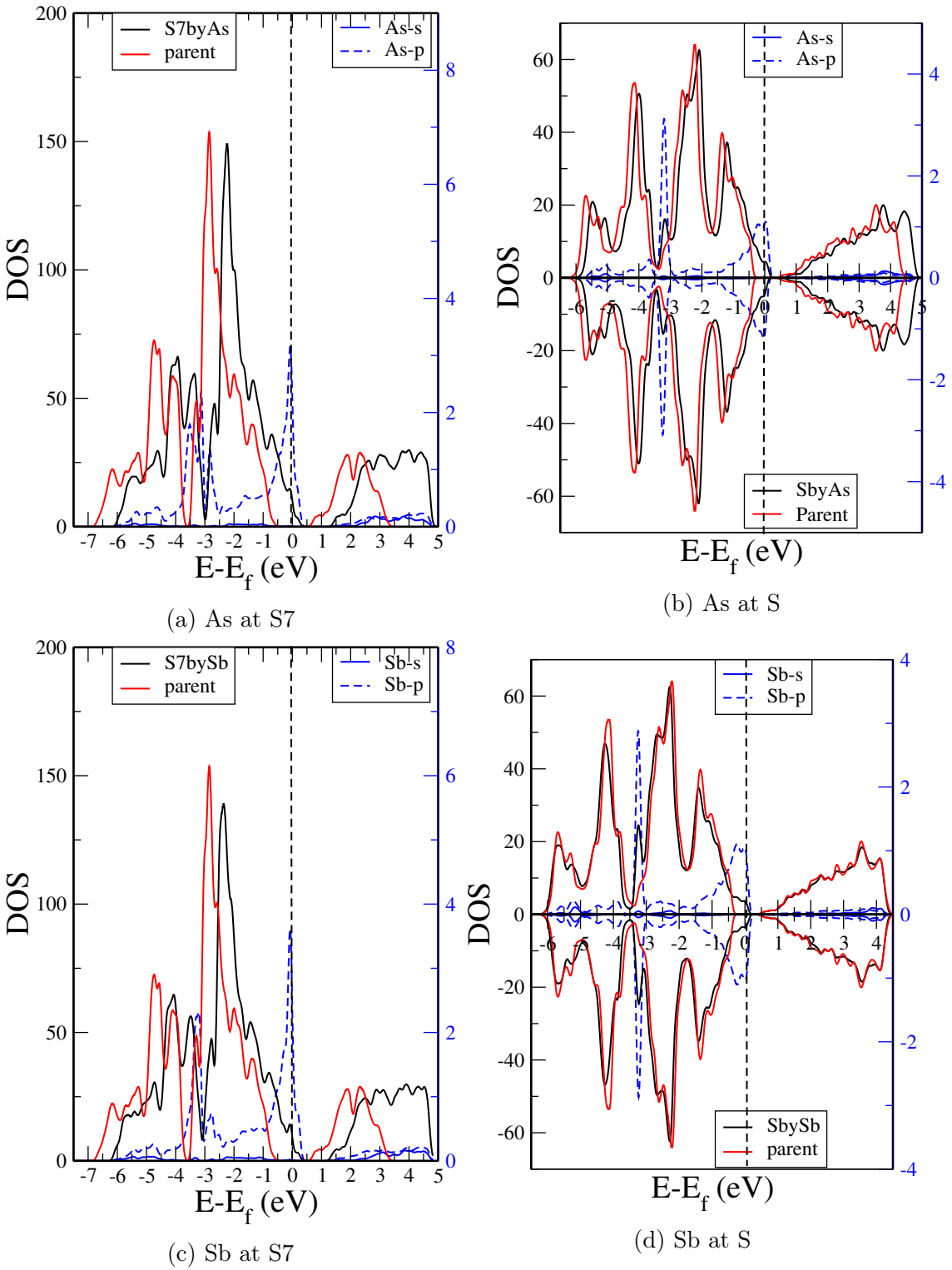


(a) As at S7

(b) As at S

(c) Sb at S7

(d) Sb at S

Figure 3.6: Group 15 Doping in $BaCu_2S_2$(-ve DOS implies down spin state)

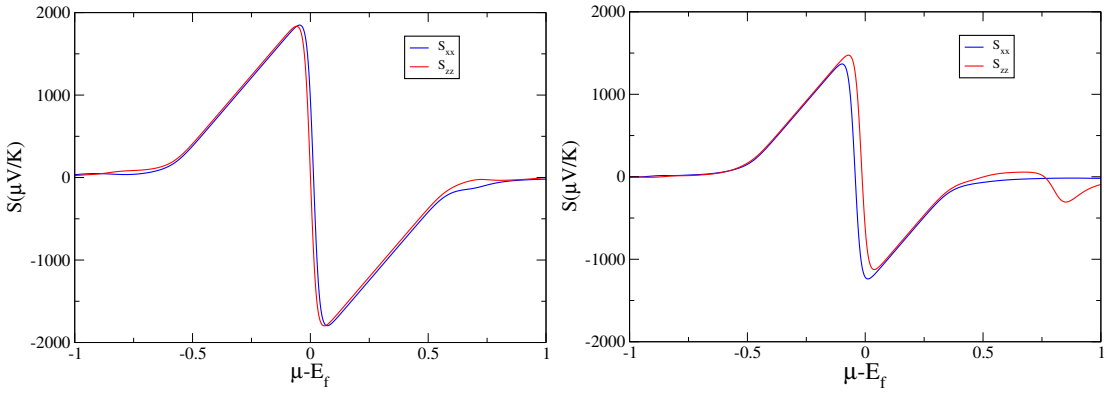


Figure 3.7: Seebeck vs chemical potential plot a:orthorhombic b:tetragonal

The effect of magnetization was quite indistinguishable between up spin and down spin(Figure:3.6(d)). For both the cases Sb acts as conventional electron acceptor.

### Comparison of different dopant

The dopant energy levels, its relative position in electronic structure, its dispersion, its peak height have been compared.
At Cu10 site in orthorhombic phase, the position of resonant peak due to p-orbital were fixed for all the group 13 dopants. But the position of the energy level due to the s-orbital varies with no general trend, from Tl's state at VB edge to Al's state closer to the bottom of the CB. Whereas at large variation in peak position, peak height can be observed on doping at Cu11 site. Behaviour of In and Ga were quite similar here, Tl showed a similar behaviour as in Cu10 site. But both the aluminium states, i.e. resonant states went into CB with no net effect in total DOS. Both the As and Sb showed similar behaviour at S7 site.
In Tetragonal phase, the energy level were much more delocalized (for group 13 dopants) owing to the greater interaction with neighbouring atoms (Cu-S bond length was smaller in tetragonal phase). In Al doping, s orbital went up in energy than p orbital, both lying in CB. In both Sb and As the new state appeared at the VB edge.

## 3.4 Transport Properties

### 3.4.1 Parent

The Transport properties relevant to a thermoelectric material were calculated for all the dopants in both the phases. The Seebeck coefficient for the parent compounds are shown in Fig. 3.7.

For tetragonal phase, the trends in transport properties are in good agreement with the reported theoretical values([7]), but the difference in the absolute value could be due to the differences in the band gap and the exchange correlation functional used. The experimental values range from 50-200 $\mu V/K$[16], depending on

the carrier concentration. Even though orthorhombic has larger thermopower than tetragonal phase, as in experimental result, the values aren't matching with the reported [16]. The effect of anisotropy doesn't have much effect in the seebeck coefficient for both the phases.

### 3.4.2 Doping

## Group 13 doping in Orthorhombic Phase

## Seebeck Coefficient

We have plotted carrier concentration vs Seebeck at 300K for both holes and electrons to study the effect of doping.

The Seebeck coefficeint for electrons as a function of carrier concentration for the orthorhombic phase is plotted in Figure 3.8. For the shown range of carrier concentration, the trends in the Seebeck coefficient can be divided into three regions: (a) Initially at the lower carrier concentration ($3\times10^{19}$ to $1.1\times10^{19}$) the Seebeck coefficient of all the dopants are larger than the parent compound, with Tl doping at Cu11 showing largest improvement. (b) Upon increasing the carrier concentration the Seebeck of all the dopants goes below the parent phase with varying degree Ga at Cu11 site having the least variation. (c) Finally at higher carrier concentration (above $8\times10^{20}$) there is a peak in the Seebeck coefficient for the doped cases while for the parent one, the Seebeck coefficient goes on decreasing (Figure 3.8). This new peak can be attributed to the resonant states introduced by the dopants. In general, doping at the Cu11 site showed minimum variation, which is due to the delocalised defect states in the conduction band.

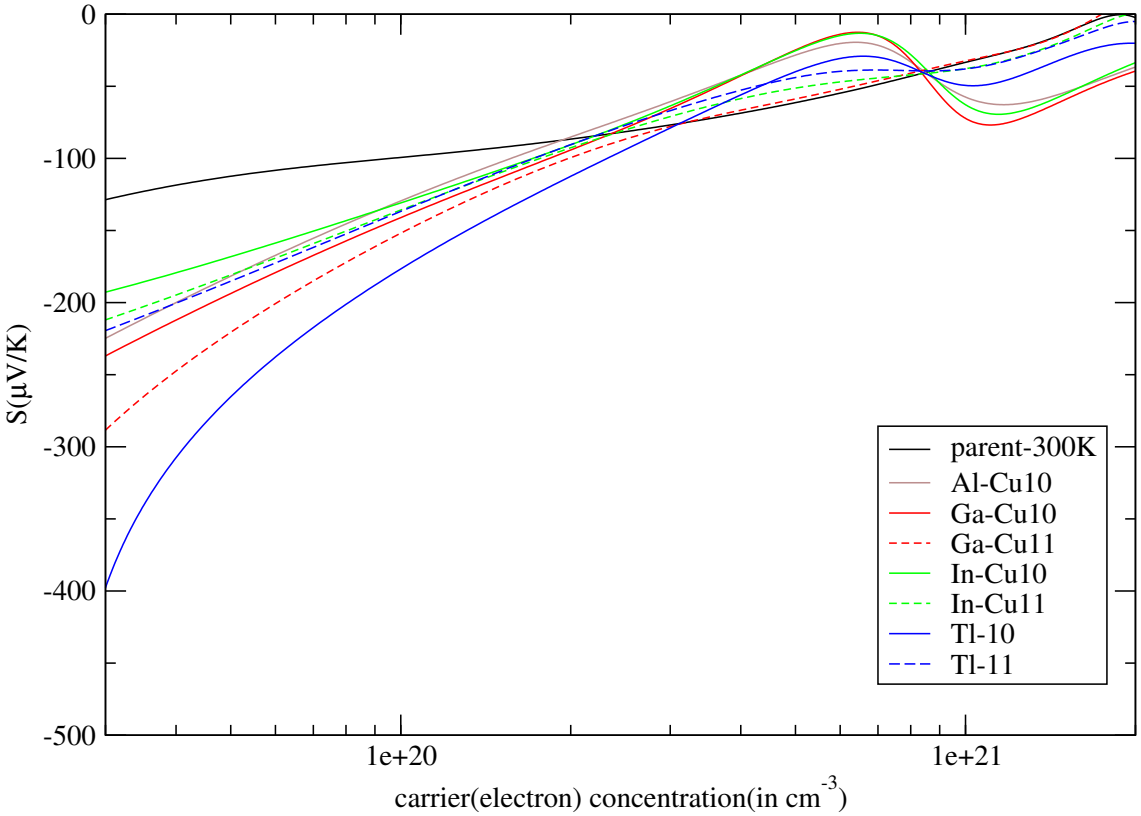


Figure 3.8: Seebeck cefficient as a function of carrier concentration for electrons in parent and doped orthorhombic $BaCu_2S_2$ at 300K.

To understand this we consider for example the case of Gallium doped at Cu10 site, two new defect states has been added below the conduction band as is evident from the band structure (Refer Supplementary material chapter). The presence of flatter defect state (from $p_z$ orbital of Ga ) at the bottom, corresponds to heavy electron whereas the bottom band of the parent has dispersion, which corresponds to lighter electron. So we can identify the improvement in Seebeck at the carrier concentration of $3\times10^{19}$ to $1.1\times10^{19}$ is due to the presence of heavier electron in the bottom of the conduction band. Dip in the Seebeck coefficient upon further increase in carrier concentration can be due to the presence of a highly dispersed state above the lowest defect state ( refer S-X direction). Subsequent increase in the Seebeck than the parent phase is due to the presence of another flatter defect band below the conduction band.

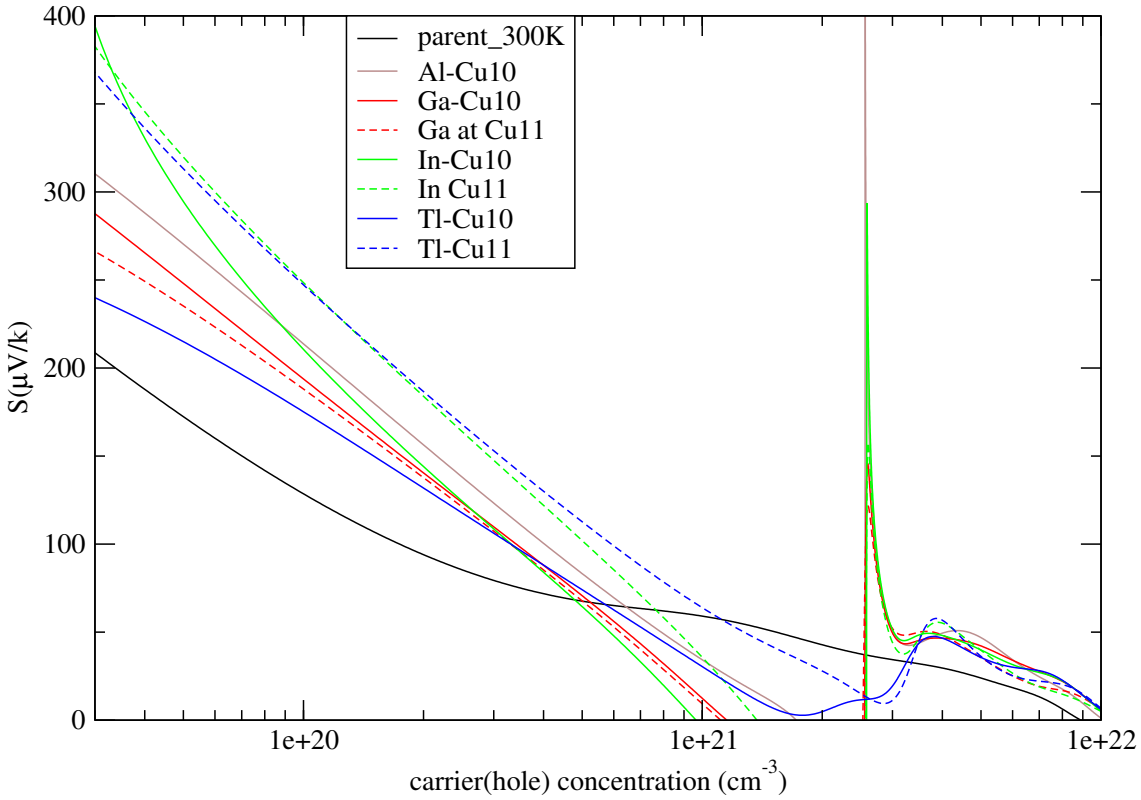


Figure 3.9: Seebeck coefficient of holes as a function of carrier concentration at 300K.

In the plot of carrier concentration of hole vs Seebeck a jump in Seebeck can be observed for a finite carrier concentration (around 2.5e21-$n_H$)3.9, which is due to the defect state detached from the VB. Since there are no states in between VB and the defect state of some of the dopant (except Tl), the Fermi function changes rapidly to zero near VB. So the discontinuity in Fermi function is causing divergence in the Seebeck coefficient giving rise to large peaks that has no physical significance. At lower carrier concentration (till $4\times10^20$ cm$^{-3}$) the Seebeck coefficients for the doped compound are larger than the parent compound. Further, beyond that it decreases till the region that contains discontinuity is reached. At a carrier concentration of about $3\times10^21$ cm$^{-3}$ the Seebeck coefficient for the doped cases show a hump, which is again a signature of resonant doping in these states.

# Chapter 4

# Conclusions and Future Outlook

In summary, we have studied the physical and electronic properties of both orthorhombic and tetragonal phases of $BaCu_2S_2$. Further, we have studied the effect of the electronic structure on doping them with Group 13 elements and two Group 15 elements, namely, Sb and As. In the orthorhombic phase the Group 13 elements occupy the Cu site and creates two defect states, one occupied and lying in the band gap while the second one empty and lies at the bottom of the conduction band. These states results in significant enhancement of the Seebeck coefficient at certain carrier concentrations, both for electrons and holes, showing signatures of resonant doping. In contrast, the Sb and As states don't create such states.

As a future outlook one needs to study the effect of dopants on the transport properties for the tetragonal phase. Also we need to study the Seebeck coefficient and other transport properties as a function of temperature. Moreover, our studies also show that for electrons the effect of resonant doping is more promising. However, this material is intrinsically hole doped due to the presence of Cu vacancies. Hence, it would be interesting to identify co-dopants that would introduce electron doping in these materials and study the effect of these on the electronic and transport properties. Additionally, a more detailed study of the transport properties needs to be performed for the doped tetragonal phase, which have also been synthesized experimentally.

# Chapter 5

# Supplementary material

## 5.1 Unfolded band structures

### 5.1.1 Group 13 dopants in Orthorhombic phase

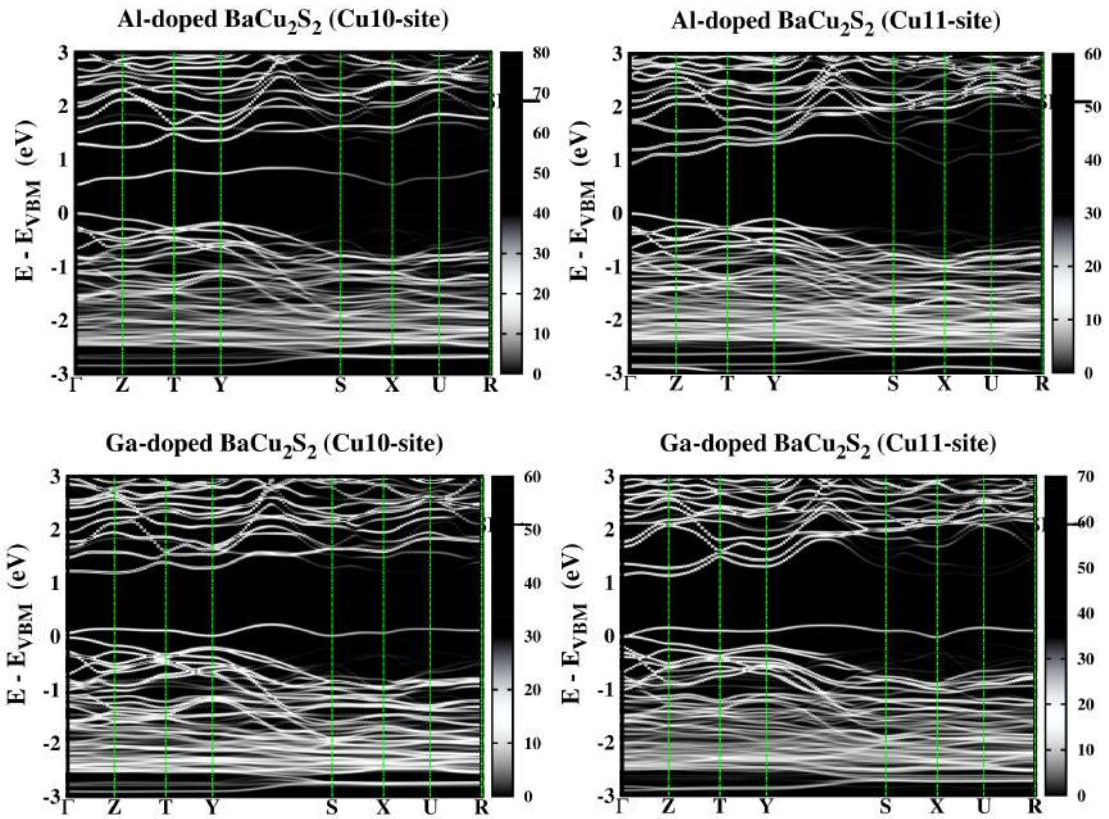

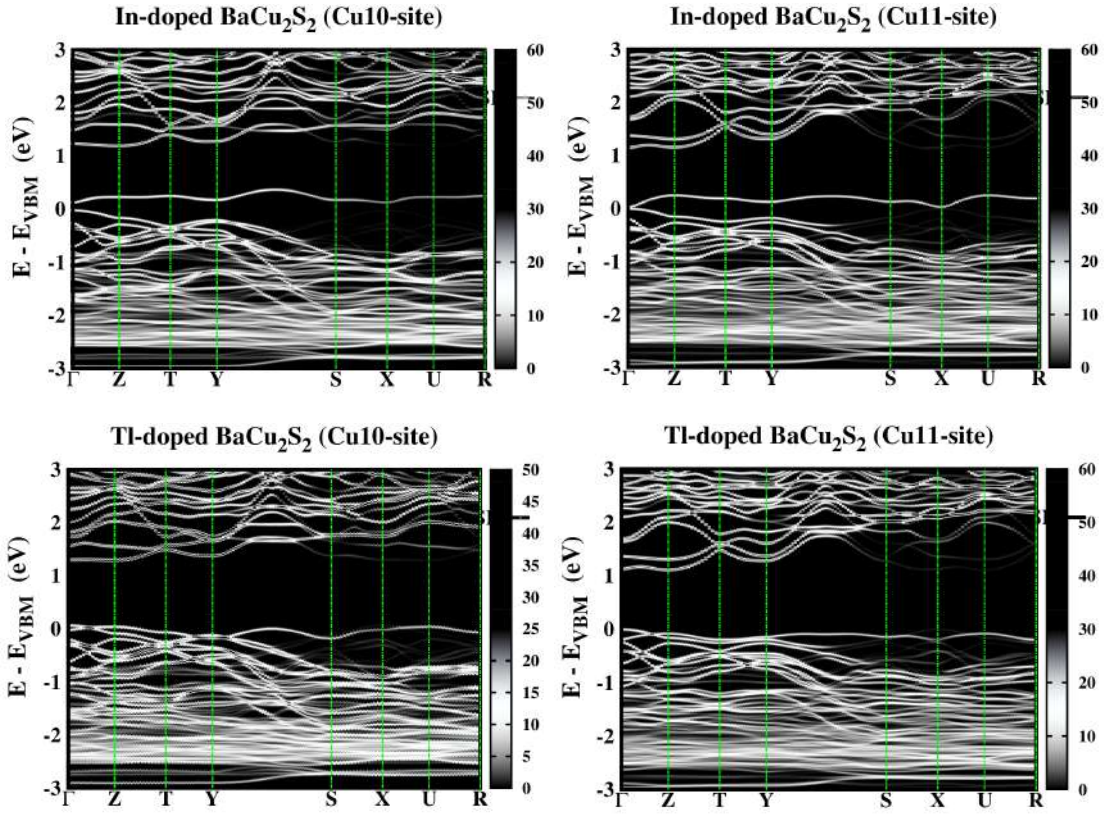
In-doped BaCu2S2 (Cu10-site)
In-doped BaCu2S2 (Cu11-site)
Tl-doped BaCu2S2 (Cu10-site)
Tl-doped BaCu2S2 (Cu11-site)
E - EVBM (eV)
Γ Z T Y S X U R

### 5.1.2 Group 13 dopants in tetragonal phase

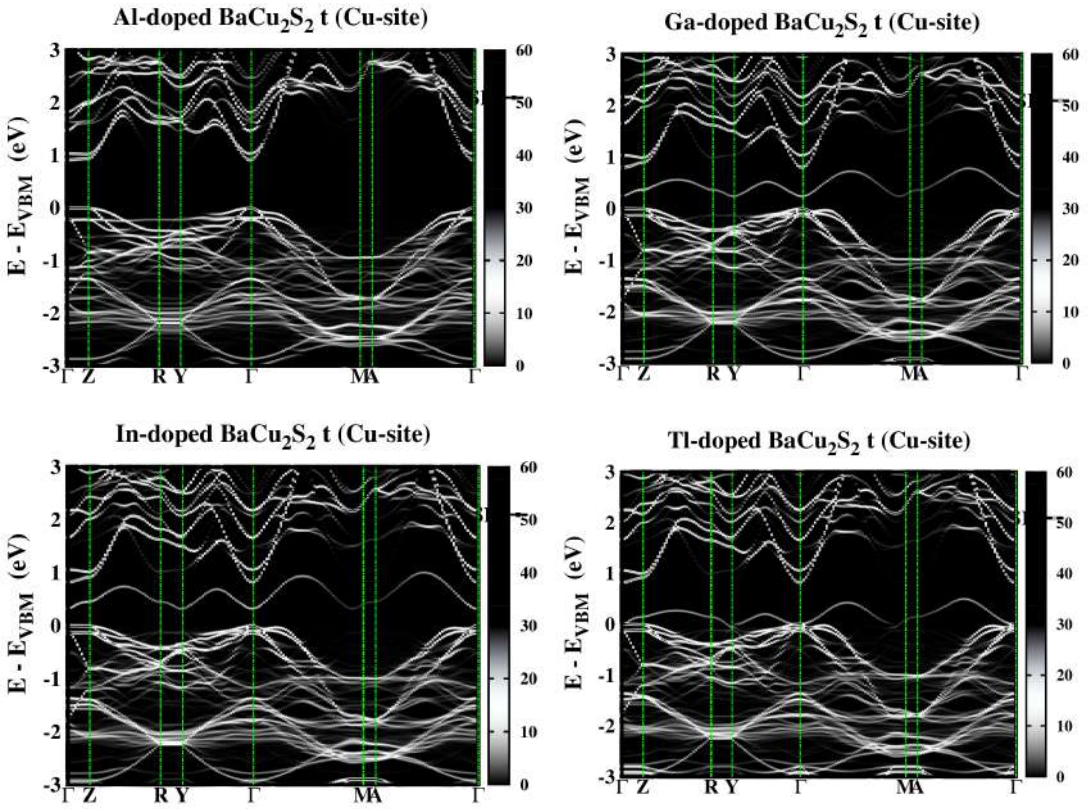

### 5.1.3 Group 15 dopants

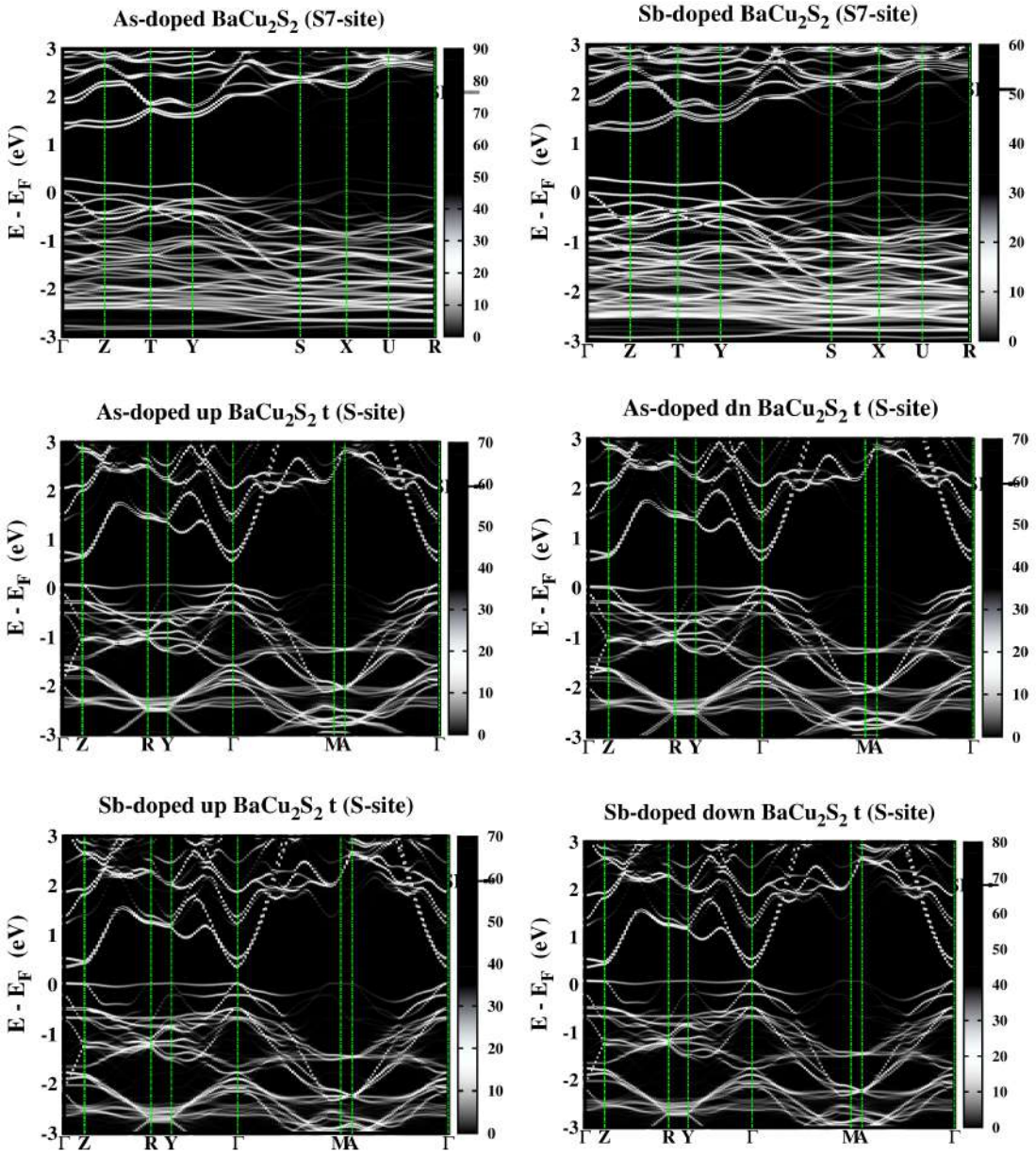

# Bibliography


[1] Felix Bloch. "Quantum mechanics of electrons in crystal lattices". In: *Z. Phys* 52 (1928), pp. 555–600.

[2] "Elementary Quantum Chemistry". In: *A Chemist's Guide to Density Functional Theory*. John Wiley & Sons, Ltd, 2001. Chap. 1, pp. 3–18. ISBN: 9783527600045. DOI: https://doi.org/10.1002/3527600043.ch1. eprint: https://onlinelibrary.wiley.com/doi/pdf/10.1002/3527600043.ch1. URL: https://onlinelibrary.wiley.com/doi/abs/10.1002/3527600043.ch1.

[3] Paolo Giannozzi et al. "QUANTUM ESPRESSO: a modular and open-source software project for quantum simulations of materials". In: *Journal of Physics: Condensed Matter* 21.39 (Sept. 2009), p. 395502. DOI: 10.1088/0953-8984/21/39/395502. URL: https://doi.org/10.1088/0953-8984/21/39/395502.

[4] Joseph P. Heremans, Bartlomiej Wiendlocha, and Audrey M. Chamoire. "Resonant levels in bulk thermoelectric semiconductors". In: *Energy Environ. Sci.* 5 (2 2012), pp. 5510–5530. DOI: 10.1039/C1EE02612G. URL: http://dx.doi.org/10.1039/C1EE02612G.

[5] P. Hohenberg and W. Kohn. "Inhomogeneous Electron Gas". In: *Phys. Rev.* 136 (3B Nov. 1964), B864–B871. DOI: 10.1103/PhysRev.136.B864. URL: https://link.aps.org/doi/10.1103/PhysRev.136.B864.

[6] J. Huster and W. Bronger. "alpha- und beta-(Ba Cu2 X2) (X = S, Se) - Darstellung von Einkristallen in Kaliumchalkogenocyanat-Schmelzen". In: *Zeitschrift fuer Anorganische und Allgemeine Chemie (1950) (DE)* 625 (1999), pp. 2033–2040.

[7] Panfei Jiao et al. "Electronic structure, thermodynamics, and thermoelectric properties of -BaCu2S2: A first-principles study". In: *Computational Materials Science* 103 (2015), pp. 105–110. ISSN: 0927-0256. DOI: https://doi.org/10.1016/j.commatsci.2015.03.018. URL: https://www.sciencedirect.com/science/article/pii/S0927025615001809.

[8] W. Kohn and L. J. Sham. "Self-Consistent Equations Including Exchange and Correlation Effects". In: *Phys. Rev.* 140 (4A Nov. 1965), A1133–A1138. DOI: 10.1103/PhysRev.140.A1133. URL: https://link.aps.org/doi/10.1103/PhysRev.140.A1133.

[9] Genady Komisarchik, David Fuks, and Yaniv Gelbstein. "High thermoelectric potential of n-type Pb1xTixTe alloys". In: *Journal of Applied Physics* 120.5 (2016), p. 055104. DOI: 10.1063/1.4960573. eprint: https://doi.org/10.1063/1.4960573. URL: https://doi.org/10.1063/1.4960573.

[10] Aditi Krishnapriyan et al. "First-principles study of band alignments in the p-type hosts BaM2X2(M= Cu, AgX= S, Se)". In: *Journal of Physics: Condensed Matter* 26.15 (Mar. 2014), p. 155802. DOI: 10.1088/0953-8984/26/15/155802. URL: https://doi.org/10.1088/0953-8984/26/15/155802.

[11] Georg K.H. Madsen and David J. Singh. "BoltzTraP. A code for calculating band-structure dependent quantities". In: *Computer Physics Communications* 175.1 (2006), pp. 67–71. ISSN: 0010-4655. DOI: https://doi.org/10.1016/j.cpc.2006.03.007. URL: https://www.sciencedirect.com/science/article/pii/S0010465506001305.

[12] G D Mahan and J O Sofo. "The best thermoelectric". In: *Proceedings of the National Academy of Sciences* 93.15 (1996), pp. 7436–7439. ISSN: 0027-8424. DOI: 10.1073/pnas.93.15.7436. eprint: https://www.pnas.org/content/93/15/7436.full.pdf. URL: https://www.pnas.org/content/93/15/7436.

[13] Richard M. Martin. *Electronic Structure: Basic Theory and Practical Methods*. Cambridge University Press, 2004. DOI: 10.1017/CBO9780511805769.

[14] Nicola Marzari et al. "Thermal Contraction and Disordering of the Al(110) Surface". In: *Phys. Rev. Lett.* 82 (16 Apr. 1999), pp. 3296–3299. DOI: 10.1103/PhysRevLett.82.3296. URL: https://link.aps.org/doi/10.1103/PhysRevLett.82.3296.

[15] T. Ohtani et al. "Electrical properties and phase transitions of TlCu3S2 and BaCu2S2". In: *Journal of Alloys and Compounds* 317-318 (2001). The 13th International Conference on Solid Compounds of Transition Elements, pp. 201–207. ISSN: 0925-8388. DOI: https://doi.org/10.1016/S0925-8388(00)01326-8. URL: https://www.sciencedirect.com/science/article/pii/S0925838800013268.

[16] T. Ohtani et al. "Electrical properties and phase transitions of TlCu3S2 and BaCu2S2". In: *Journal of Alloys and Compounds* 317-318 (2001). The 13th International Conference on Solid Compounds of Transition Elements, pp. 201–207. ISSN: 0925-8388. DOI: https://doi.org/10.1016/S0925-8388(00)01326-8. URL: https://www.sciencedirect.com/science/article/pii/S0925838800013268.

[17] Zhenyu Pan and Heng Wang. "A descriptive model of thermoelectric transport in a resonant system of PbSe doped with Tl". In: *J. Mater. Chem. A* 7 (20 2019), pp. 12859–12868. DOI: 10.1039/C9TA02670C. URL: http://dx.doi.org/10.1039/C9TA02670C.

[18] Robert G. Parr. "Density Functional Theory of Atoms and Molecules". In: *Horizons of Quantum Chemistry*. Ed. by Kenichi Fukui and Bernard Pullman. Dordrecht: Springer Netherlands, 1980, pp. 5–15. ISBN: 978-94-009-9027-2.

[19] M. C. Payne et al. "Iterative minimization techniques for ab initio total-energy calculations: molecular dynamics and conjugate gradients". In: *Rev. Mod. Phys.* 64 (1992), pp. 1045–1097. DOI: 10.1103/RevModPhys.64.1045.

[20] Yanzhong Pei et al. "Convergence of electronic bands for high performance bulk thermoelectrics". In: *Nature* 473.7345 (2011), pp. 66–69. DOI: 10.1038/nature09996.

[21] John P. Perdew, Kieron Burke, and Matthias Ernzerhof. "Generalized Gradient Approximation Made Simple [Phys. Rev. Lett. 77, 3865 (1996)]". In: *Phys. Rev. Lett.* 78 (7 Feb. 1997), pp. 1396–1396. DOI: 10.1103/PhysRevLett.78.1396. URL: https://link.aps.org/doi/10.1103/PhysRevLett.78.1396.

[22] Kristin Persson. *Materials Data on Ba(CuS)2 (SG:62) by Materials Project*. An optional note. July 2014. DOI: 10.17188/1277207.

[23] Voicu Popescu and Alex Zunger. "Extracting $E$ versus $\overset{P}{k}$ $effectivebandstructurefromsupercellcalculationsonalloysandimpurities$". In: *Phys. Rev. B* 85 (8 Feb. 2012), p. 085201. DOI: 10.1103/PhysRevB.85.085201. URL: https://link.aps.org/doi/10.1103/PhysRevB.85.085201.

[24] D.M. Rowe. *CRC Handbook of Thermoelectrics (1st ed.(Ed.). (1995)*. CRC Press. DOI: 10.1201/9781420049718.

[25] Umar Abubakar Saleh et al. "Evaluation of a PV-TEG Hybrid System Configuration for an Improved Energy Output: A Review". In: *International Journal of Renewable Energy Development* 10.2 (2021).

[26] G.A. Slack. "Nonmetallic crystals with high thermal conductivity". In: *Journal of Physics and Chemistry of Solids* 34.2 (1973), pp. 321–335. ISSN: 0022-3697. DOI: https://doi.org/10.1016/0022-3697(73)90092-9. URL: https://www.sciencedirect.com/science/article/pii/0022369773900929.

[27] "The Hohenberg-Kohn Theorems". In: *A Chemist's Guide to Density Functional Theory*. John Wiley & Sons, Ltd, 2001. Chap. 4, pp. 33–40. ISBN: 9783527600045. DOI: https://doi.org/10.1002/3527600043.ch4. eprint: https://onlinelibrary.wiley.com/doi/pdf/10.1002/3527600043.ch4. URL: https://onlinelibrary.wiley.com/doi/abs/10.1002/3527600043.ch4.

[28] "The Kohn-Sham Approach". In: *A Chemist's Guide to Density Functional Theory*. John Wiley & Sons, Ltd, 2001. Chap. 5, pp. 41–64. ISBN: 9783527600045. DOI: https://doi.org/10.1002/3527600043.ch5. eprint: https://onlinelibrary.wiley.com/doi/pdf/10.1002/3527600043.ch5. URL: https://onlinelibrary.wiley.com/doi/abs/10.1002/3527600043.ch5.

[29] Jos Thijssen. *Computational Physics*. 2nd ed. Cambridge University Press, 2007. DOI: 10.1017/CBO9781139171397.

[30] Lihua Wu et al. "Resonant level-induced high thermoelectric response in indium-doped GeTe". In: *NPG Asia Materials* 9.1 (2017). DOI: 10.1038/am.2016.203.